Tanimoto and Anderson
Progress in Earth and Planetary Science (2023) 10:56
https://doi.org/10.1186/s40645-023-00587-7

Progress in Earth and Planetary Science

REVIEW

Open Access

Seismic noise between 0.003 Hz and 1.0 Hz and its classification

Toshiro Tanimoto[1*] and Aaron Anderson[1]

Abstract

It is now established that the primary microseism, the secondary microseisms, and the hum are the three main components of seismic noise in the frequency band from about 0.003 Hz to 1.0 Hz. Monthly averages of seismic noise are dominated by these signals in seismic noise. There are, however, some temporary additional signals in the same frequency band, such as signals from tropical cyclones (hurricanes and typhoons) in the ocean and on land, storm-quakes, weather bombs, tornadoes, and wind-related atmospheric pressure loading. We review these effects, lasting only from a few hours to a week but are significant signals. We also attempt to classify all seismic noise. We point out that there are two broad types of seismic noise, the propagating seismic waves and the quasi-static deformations. The latter type is observed only for surface pressure changes at close distances. It has been known since about 1970 but has not been emphasized in recent literature. Recent data based on co-located pressure and seismic instruments clearly show its existence. Because the number of phenomena in the first type is large, we propose to classify all seismic noise into three categories: (1) propagating seismic waves from ocean sources, (2) propagating seismic waves from on-land sources, and (3) quasi-static deformation at ocean bottom and on land. The microseisms and the hum are in the first category although there are differences in the detailed processes of their excitation mechanisms. We will also classify temporary signals by these categories.

Keywords Low-frequency seismic noise, Ocean–solid earth interaction, Wave–wave interaction, Quasi-static deformation

1 Introduction

The study of seismic noise started shortly after mechanical seismic instruments were developed in the late nineteenth century to the early twentieth century (e.g., Wiechert 1904; Gutenberg 1912; Omori 1918; Bernard 1990). It was noted that the microseisms were the dominant signals in the absence of earthquake signals, even in these early seismic instruments. The cause of excitation was not clear but early postulates included the excitation by surf breaking on coasts (Wiechert 1904) and ocean swell (Omori 1918), which we now know to be correct for some microseism sources. However, it took almost a half-century before the basic mechanisms for the microseisms were sorted out by Hasselmann (1963). This was mainly because the cause of the secondary microseism was not properly understood until the work of Longuet-Higgins (1950). Gutenberg, who wrote a doctoral thesis in Göttingen on seismic noise (Gutenberg 1912), stated twenty-four years later (Gutenberg 1936) "while for most of the types of microseisms the cause is known, there is still no agreement among seismologists on the cause of the most common type, namely, the more or less regular microseisms with periods of from 4 to 10 s." The double-frequency mechanism for the secondary microseism in which the interactions between ocean waves generate seismic noise was the missing element for many decades in the early twentieth century. Clarification of this process due to the nonlinear interactions among ocean

*Correspondence:
Toshiro Tanimoto
toshirotanimoto@ucsb.edu
[1] Department of Earth Science and Earth Research Institute, University of California, Santa Barbara, CA 93106, USA

waves was finally published by Longuet-Higgins (1950). This paper also referred to an earlier, equivalent work by Miche (1944) which was written in French. This led to a summary of excitation mechanisms for seismic noise by Hasselmann (1963).

Based on Hasselmann's (1963) analysis, it has been stated (e.g., Ardhuin et al. 2015) that the two main mechanisms of excitation of microseisms, the direct interactions between ocean waves and solid Earth near the coast, and the interactions among the ocean waves can explain the excitation of the microseisms. Verification of these mechanisms was not straightforward in the 1960s and 1970s, however, because the widely analyzed seismic data during these decades came from the World Wide Standardized Seismograph Network (WWSSN) stations, which had two different sensors, covering the short periods (targeted at about 1 s) and the long periods (target at about 15 s) separately. These sensors were precisely designed to avoid the large microseism noise between these periods and prevented further analysis of seismic noise. This situation changed, however, when the digital, continuous recordings of broadband instruments became common in the mid-1980s, especially with the formation of the Incorporated Research Institutions of Seismology (IRIS Science Plan 1984).

In this paper, we limit our discussion to seismic noise in the low-frequency band from about 0.003 Hz to 1.0 Hz. We have learned from the past few decades that the dominant causes of seismic noise between about 0.003 Hz and 1.0 Hz are the processes in the oceans (e.g., Nishida 2017). Below 0.003 Hz, seismic noise is primarily controlled by atmospheric processes (e.g., Warburton and Goodkind 1977; Zürn and Widmer 1995; Beauduin et al. 1996; Tanimoto 1999; Roult and Crawford 2000; Tanimoto et al. 2015a, b). Therefore, seismic noise below about 1 Hz is primarily caused by nature rather than anthropological processes.

Above 1.0 Hz, there is noise generated by nature such as winds and ocean processes, but various forms of human activities contribute greatly. Examples include the resonant frequencies of buildings (except for the true high-rises) that are typically above 1 Hz and the noise from trains, automobiles (highways), factories, and other human activities. The high-rise buildings that have ~ 100 stories have resonant periods of the order of 10 s and are an exception to this statement, but such buildings are still quite rare.

The importance of human-generated seismic noise for frequencies above 1 Hz became abundantly clear during the COVID-19 lockdown periods in the past few years (e.g., Lecocq et al. 2020; Xiao et al. 2020). We found extremely quiet periods in seismic noise for frequencies above 1 Hz. This was a new confirmation of the importance of human-related, cultural noise above 1.0 Hz. There are other fascinating aspects of seismic noise above 1.0 Hz, but in this paper, we restrict the frequency range to below 1 Hz and focus only on seismic noise caused by nature.

We have two main goals for this paper. One is to summarize various types of seismic noise, not only the three main types of noise between 0.003 and 1.0 Hz but seven relatively short-term deviations from them. The other goal is to classify the entire set of seismic noise.

In Sect. 2, we summarize the main three components of seismic noise, the primary microseism, the secondary microseism, and the hum, even though there already exist reviews on them such as Nishida (2017) and Tanimoto et al. (2015a, b). We will try to put them in context for this paper in order to discuss the different types of noise.

In Sect. 3, we first discuss that the entire seismic noise can be classified into two broad types: the first type is the propagating seismic noise and the second type is the quasi-static deformation. The latter type is generated by slow surface pressure changes near a station that act like a surface load. The solid Earth deforms almost statically in response to slow surface pressure changes in time. For our classification scheme, because there are many examples of seismic noise for the first type, we will introduce a subdivision in it and attempt to classify seismic noise by three categories: (1) propagating seismic waves from ocean processes, (2) propagating seismic waves from atmospheric processes, and (3) the quasi-static deformation from pressure loading at ocean bottom and on land. In Sect. 4, we will discuss seven phenomena that are deviations from the main three noises and classify them according to this scheme.

In Sect. 5, we will visit some long-lasting questions from the perspective of our current understanding of seismic noise. We believe that a question on microseisms such as "Are the sources coastal or pelagic?" (Haubrich and McCamy 1969) can now be answered. We also review recent literature on the reason why SH-type waves (Love waves) are observed in the frequency band of secondary microseism (0.1–0.4 Hz); this appears puzzling because the wave–wave interaction at the source is equivalent to vertical forcing and thus cannot excite SH-type waves.

2 Review

In this section, we review the three main components of seismic noise, the primary microseism, the secondary microseism, and the hum. There is significant overlap with previous publications such as Nishida (2017) and Tanimoto et al. (2015a) but to define and clarify some terms for later use we will discuss these phenomena in detail.

2.1 The primary and the secondary microseisms

We start our discussion with the well-known new-low-noise-model (NLNM) by Peterson (1993) which summarized the characteristics of seismic noise. Figure 1 shows this model that plots the power spectral densities (PSD) of ground acceleration as a function of frequency from 0.1 mHz (milli-hertz) to 10 Hz. The largest peak in Fig. 1 is the secondary microseism whose frequency range is approximately between 0.1 and 0.4 Hz. The small peak at about 0.05–0.07 Hz that shows up on the lower frequency side (left) of this peak is the primary microseism. It has been confirmed by many studies (e.g., Bromirski, et al. 1999) that the frequencies of the primary microseism match with those of ocean waves from ocean buoy data, and the frequencies of the secondary microseism are approximately twice the frequency of ocean waves (hereafter, the double frequency or DF).

The frequency range of the secondary microseism slightly differs from location to location, especially the width of the main frequency band. Figure 2 shows examples from three locations; YBH (Fig. 2a) in Northern California, HRV in Massachusetts, USA (Fig. 2b), and CTAO in the Northwest region of Australia (Fig. 2c). Many seismic stations in California, such as YBH, show that the secondary microseism has a peak at about 0.15 Hz which is approximately double the ocean-wave frequency. Its width is typically limited to the range between 0.1 and 0.25 Hz (Fig. 2a, YBH). On the other hand, many stations on the east coast of the United States (Fig. 2b, HRV) generally show a broader secondary-microseism peak spanning from about 0.1 Hz to 0.4 Hz. Stations in the northwest U.S. in the states of Washington and Oregon,

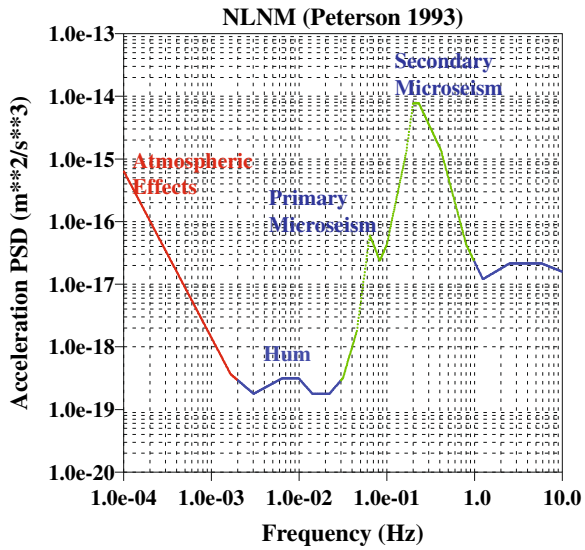

Fig. 1 Characteristic spectral features of seismic noise from 0.0001 to 10 Hz. This is a model (NLNM) by Peterson (1993). For frequencies below 0.003 Hz, atmospheric processes are the main source of seismic noise but oceanic processes are the main source in the frequency band from 0.003 to 1.0 Hz; there are three main seismic noises in this frequency band and they are, from low frequency, the hum, the primary microseism and the secondary microseism

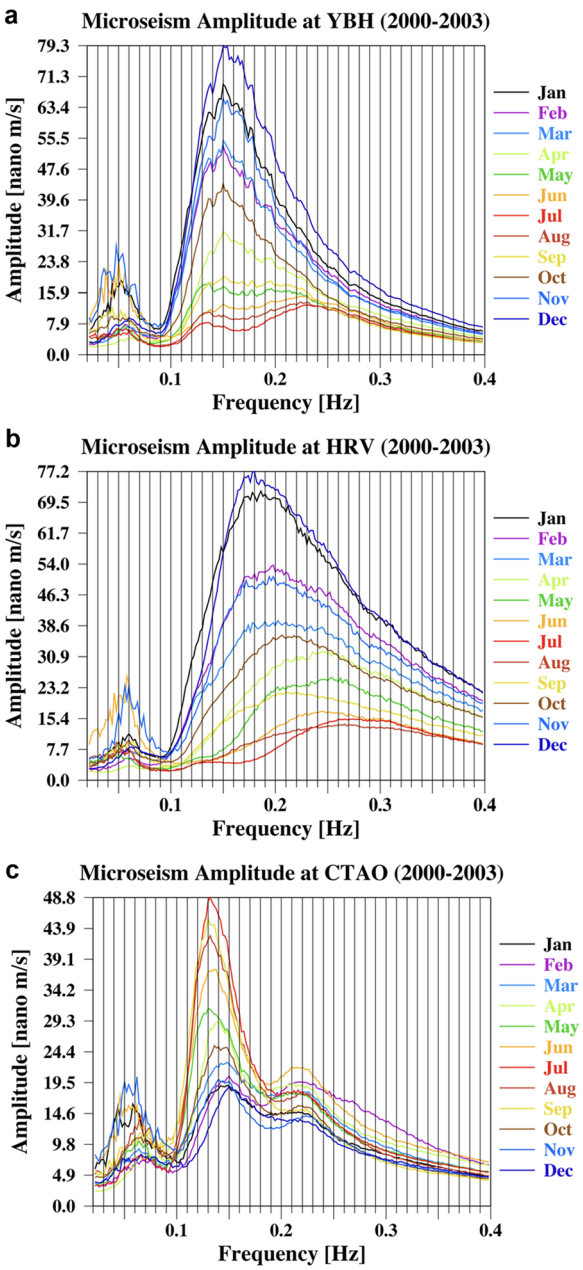

Fig. 2 Spectral characteristics of primary microseism and secondary microseism at three locations, YBH in California, USA (top), HRV near the east coast of USA (middle), and CTAO in the northeastern part of Australia (bottom). Monthly averages are shown in different colors. Spectral shapes of the secondary microseism (0.1–0.4 Hz) vary greatly from location to location which in most cases reflect the behavior of ocean waves in the nearby ocean

also show a similar broad peak in comparison to California stations. Such a variation in the width of the secondary microseism also occurs in the southern hemisphere (Fig. 2c, CTAO in Australia), although the high-amplitude season is the winter in each hemisphere. These high-amplitude seasons occur when ocean waves in the nearby oceans have high amplitudes, suggesting that the source of secondary microseisms is dominated by ocean waves from the nearby ocean (Bromirski et al. 1999).

Koper and Burlacu (2015) pointed out, using seismic data from the Transportable Array of the EarthScope network (hereafter TA), that the secondary microseism (DF) consisted of two peaks, the lower frequency peak at about 0.1–0.17 Hz (period 6–10 s) and the higher frequency peak at about 0.17–0.5 Hz (period 2–6 s). Polarization analysis indicated that their source areas point to different oceanic regions and their sources generally agreed with the oceanic noise source model of Ardhuin et al. (2011). The source regions of seismic noise in the oceans have slightly different spectral peaks. The station they analyzed in the paper was a TA station in Utah which is located far away from the Pacific Ocean and the Atlantic Ocean. If a station were close to the coast, however, seismic noise would be strongly influenced by the ocean-wave characteristics in the nearby ocean and less so from other distant oceans. However, there could be short time intervals even for stations in California for which the excitation source in the Atlantic Ocean is the cause of seismic noise when the nearby ocean becomes calm (Schulte-Pelkum et al. 2004).

2.2 Forcing mechanisms of primary and secondary microseisms

2.2.1 Excitation of primary microseism and direct interaction between ocean waves and solid earth (DI)

The reason that ocean waves and the primary microseism have the same frequency is because the ocean waves directly interact with the seafloor and exert forces on the solid Earth. In the case of primary microseism, ocean waves are the swells that are generated by storms (low-pressure systems) at distant locations, usually in the middle of oceans. Figure 3a, b show an example of an ocean swell that was generated in the Northern Pacific Ocean. Ocean wave heights (Significant Wave Height, SWH) are shown in Fig. 3a, displaying more than 6 m of maximum amplitude (dark red). These waves were generated in the mid-latitude region of the Northern Pacific Ocean and propagated toward the west coast of the U.S.

These waves, typically at periods of about 14 s but occasionally becoming longer periods of up to about 18 s, do not generate seismic waves while they are in deep oceans. This can be understood easily if we examine the wavelength and the depth extent of these waves. The dispersion relation of these ocean waves (in deep water meaning $\tanh(kH) \approx 1$) is given by $\omega^2 = gk$ where $\omega (= 2\pi f)$ is the angular frequency (f is the frequency in Hz), $g\left(= 9.8 \frac{m}{s^2}\right)$ is gravitational acceleration, $k (= \frac{2\pi}{\lambda})$ is the wavenumber and λ is the wavelength. Rewriting this relation in terms of the wavelength, we can write it as $\lambda = g/(2\pi) \times T^2 \approx 1.56 T^2$. Using a typical period $T = 14$ (s), $\lambda = 306$ (m), which is the horizontal wavelength. These waves are surface waves in the ocean and their amplitudes decay exponentially with depth. Therefore, the predominant oscillating parts of these waves may reach about 200 m but not beyond. Therefore, in open oceans where ocean depths are typically 3–4 km, they cannot possibly interact with the solid Earth. Consequently, no excitation of seismic waves can occur by those propagating waves in one direction (Longuet-Higgins 1950).

When the swells reach near the coasts, ocean depths become shallow enough for ocean-wave energy to interact with the seafloor. Figure 3c indicates a possible location of seismic waves near the coast, indicated by 1. If there is a continental shelf region near the coast, this interaction occurs within the shelf with ocean depths of less than about 200 m.

This process of direct interaction may also be viewed as the scattering of seismic waves. Propagating ocean waves are a particular mode of surface waves. If the Earth were layered and laterally homogeneous, it would maintain its mode types and remain orthogonal to other modes. But once their motions reach the ocean floor, either due to topography on the ocean floor or shallow and sloping coastal structure, some portions of their energy get converted to other types of seismic waves by the scattering process. This process can produce Rayleigh and Love waves as well as body waves such as P waves and S waves.

2.2.2 Excitation of the secondary microseism by the wave–wave interaction

2.2.2.1 The Longuet-Higgins pressure formula The mechanism for the excitation of secondary microseism is entirely different and ocean waves do not need to directly interact with the solid Earth. In Fig. 3c we indicate a possible location as 2, but the excitation can occur anywhere in the ocean. The only condition is that two ocean waves that propagate in an opposite direction must meet (or collide). Then, through the nonlinear term in the Navier–Stokes equation, an equivalent vertical force results from this interaction; more explicitly, the origin of this effect is the second term on the lefthand side of the Navier–Stokes equation:

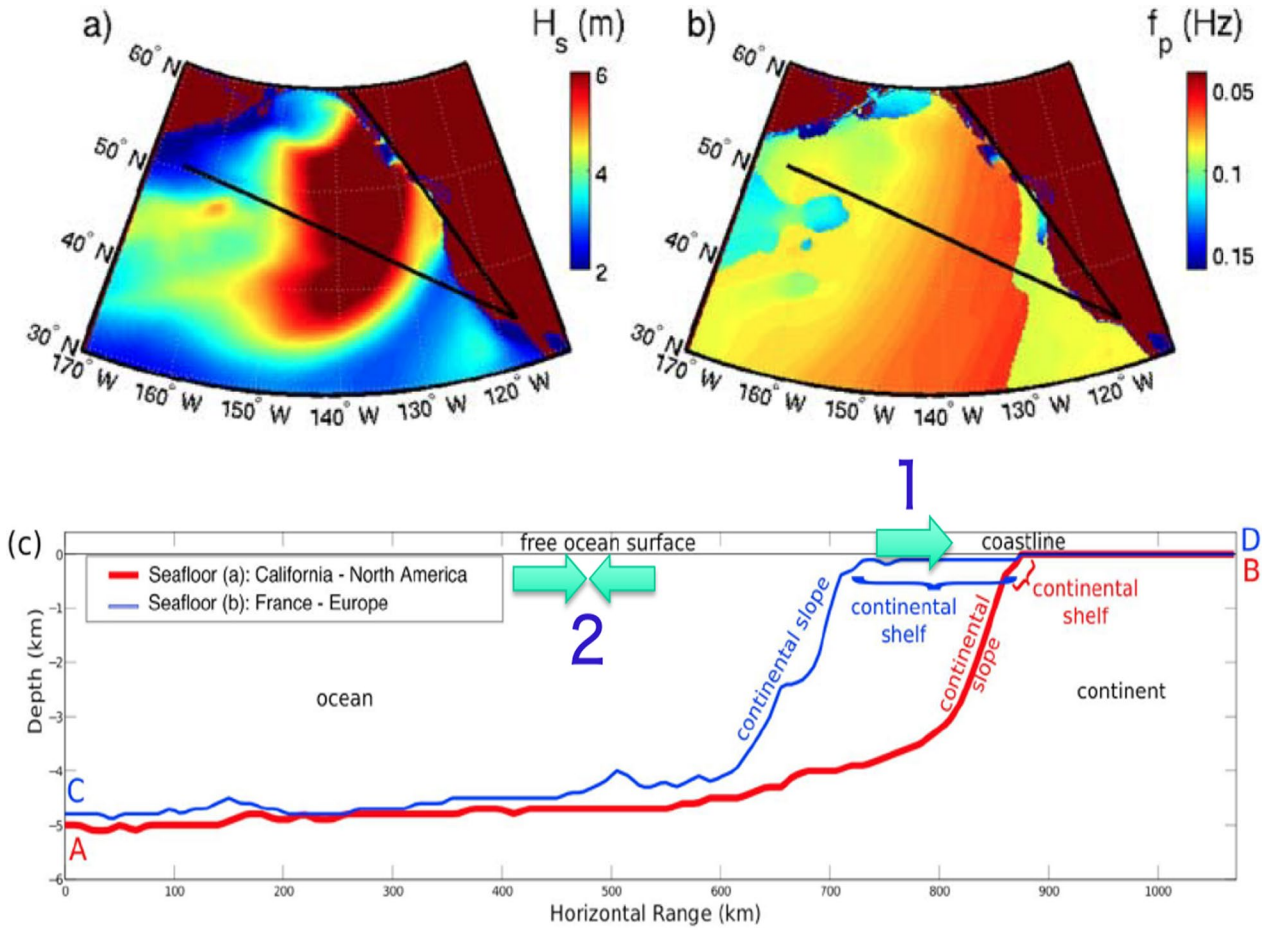

Fig. 3 **a** Significant wave height of the swell that was generated in the northern part of the Pacific Ocean. The northernmost portion has hit the coast of Canada and it is propagating toward the east. **b** Dispersive character of the swell is depicted as it is propagating toward the east. The lower frequency energy is at its front (red region). **c** The wave–wave interactions can occur in the ocean of any depth such as 2 in this figure but the direct interaction can only occur in shallow ocean depths such as 1, usually a location very close to the coast. This is after Gualtieri et al. (2015)

$$\rho\frac{\partial \mathbf{v}}{\partial t} + \rho(\mathbf{v}\cdot\nabla)\mathbf{v} = -\nabla P - \rho\mathbf{g} \tag{1}$$

where ρ is density, $\mathbf{v}$ is velocity, P is pressure and $\mathbf{g}$ is gravitational acceleration. We drop the viscous term because it is not important in our discussion.

Longuet-Higgins (1950) showed that when two ocean waves that propagate in an opposite direction meet, it generates pressure given by

$$P = \frac{1}{2}\frac{\partial^2}{\partial t^2}\overline{\zeta^2} \tag{2}$$

where ζ is the ocean surface displacement and the bar indicates spatial averaging over a large region whose scale is much larger than the wavelength of ocean waves. For example, if we take a case of two cosine waves that propagate in opposite directions, we have

$$\zeta = a_1\cos(\omega t - kx) + a_2\cos(\omega t + kx) \tag{3}$$

Substituting (3) in (2), we get.

$$P = -2\rho\omega^2 a_1 a_2 \cos(2\omega t), \tag{4}$$

where P is proportional to a_1a_2 and has twice the frequency of ocean waves that collided. The depth extent of ocean waves may be confined to the upper 100–200 m from the ocean surface for the relevant frequency range of 0.05–0.07 Hz (ocean swell frequencies) but Eq. (4) shows that this pressure is associated with a standing wave and can exert pressure at any depth under the location where two waves meet. The important point is that this process can generate seismic waves in the ocean of any depth. This process is often termed the wave–wave interaction process.

The wave–wave interaction can happen in the neighborhood of a low-pressure (weather) system in open oceans as the center of the low-pressure system moves. Teleseismic P-wave sources are now commonly identified near a tropical cyclone (hurricane and typhoon) which can be explained best by the wave–wave interaction. It can also occur near a coast because the incoming ocean waves can reflect from the coast and meet the incoming waves after their reflection. The latter near-coast case can be verified quantitatively by comparing the amplitudes of the primary microseism and those of the secondary microseism. Near the coast, the amplitude of a reflected wave may be written as αA, where α is the reflection coefficient. Then the above pressure term becomes proportional to $P \propto \alpha A^2$. It means that if the amplitude of the primary microseism is A, the amplitude of the secondary microseism should be *proportional to* A^2. This relation was verified in Nishida (2017) for stations near the coasts. However, for locations far away from the coast this relation becomes obscure. This is probably because propagation across the complex continental structures in the crust from the coast to an in-land seismic station can mask the distinct amplitude characteristics due to scattering during the propagation of waves.

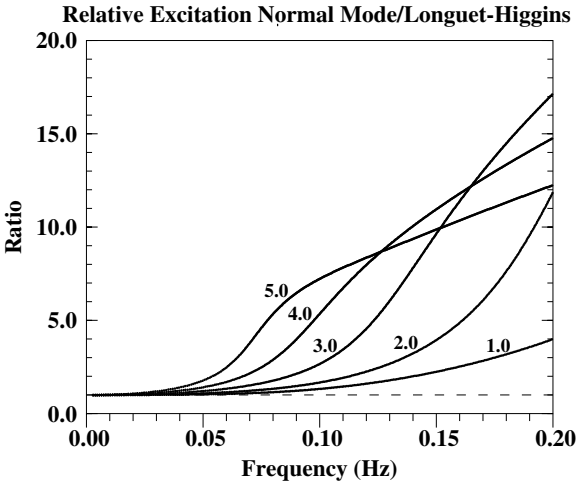

Fig. 4 The relative size of the excitation of Rayleigh waves between the normal mode theory and the Longuet-Higgins formula. The five lines are for different ocean depths from 1 to 5 km. At low frequencies, the ratio approaches 1 and shows quantitative agreement. At frequencies of the secondary microseism, they differ but that is because the formula (Eqs. 2 or 4 in the text) does not contain the depth resonance effects. Longuet-Higgins (1950) discussed this depth effect which was correctly used by Kedar et al. (2008) and Ardhuin et al. (2011)

2.2.2.2 Modal excitation theory and the effects of ocean depth Longuet-Higgin's (1950) derivation for pressure is relatively intuitive and is often used to explain the wave–wave interaction mechanism. Simply stated, the double-frequency standing waves are generated by colliding ocean waves and create pressure change at the seafloor. But we can also analyze this excitation problem as a modal excitation problem. The modal excitation by the nonlinear term in (1) was analyzed by Tanimoto (2007a), following the normal mode excitation theory (e.g., Gilbert 1970; Aki and Richards 2002; Dahlen and Tromp 1998). The results confirmed that a term equivalent to the above pressure term emerges through the analysis. However, the quantitative match required consideration of the frequency range and the ocean depth. For the frequency range 0.05–0.07 Hz, if the ocean depth were 1 km or less, Fig. 4 shows that Longuet-Higgin's pressure term and the modal excitation theory agree almost perfectly. But if the ocean were deeper, the modal excitation theory predicted a more efficient excitation than that predicted by the Longuet-Higgins formula. For an ocean depth of 5 km, an equivalent force was larger by a factor of five (Tanimoto 2007b).

But this is not a fair comparison as the effects from ocean depth are not included in (4). The effects from ocean depth are related to the resonant effects within the oceanic layer. Longuet-Higgins (1950, p. 34) stated that "the microseism amplitudes may be increased by a factor of order 5 owing to the greater response of the physical system for certain depths of water." In other words, the excitation may be enhanced due to resonant effects if the ocean depth is close to $\frac{1}{2}(m-1)+1/4$ of an acoustic wavelength in water, where m is an integer related to the number of reverberations in the ocean (Kedar et al. 2008). The modal excitation approach contains such effects automatically. The inclusion of ocean-depth effects with the above pressure term in (2) resolves this problem and in most applications such effects are taken into account (Kedar et al. 2008; Ardhuin and Herbers 2013; Ardhuin et al. 2011; Gualtieri et al. 2015).

2.3 Hum: background oscillations

2.3.1 Discovery

The frequency range of the hum is approximately from about 3 mHz to 15 mHz. An example of spectra, stacked from 15 global broadband stations (Tanimoto 2005), is shown in Fig. 5 (top). Spectral peaks of individual fundamental spheroidal modes are clear from about 3 mHz to 8 mHz but the broad background spectra that span in frequency from about 3 mHz to 15 mHz have a peak at about 9 mHz. An arrow is shown to indicate this broad peak. This peak had already been recognized by Peterson (1993, Fig. 1). The boxed part in the top figure is enlarged in the bottom panel and the spectra confirm that each peak is a fundamental spheroidal mode. The reason that each spheroidal mode peak cannot be seen above 8 mHz should be partly due to attenuation. It can

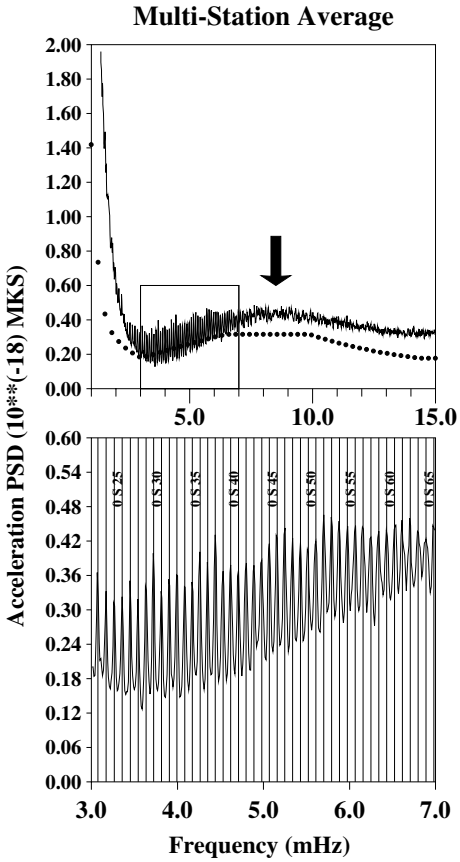

Fig. 5 An example of the hum signals, obtained from stacking of 15 global seismic stations. Peterson's (1993) low noise model, NLNM, is shown by dots in the top panel. A small box in the top panel is enlarged in the bottom panel. Vertical lines in the bottom panels show the eigenfrequencies of fundamental spheroidal modes of PREM. There are individual peaks of spheroidal modes between about 2 mHz and 8 mHz but the entire spectral bump from 2 to 15 mHz is the hum, mostly consisting of globally circulating Rayleigh waves

also be because of contributions from smaller sources in which only minor-arc Rayleigh waves are observed. Observation of modal peaks in spectra requires not only minor-arc Rayleigh waves but also great-circling Rayleigh waves that circulated the Earth a few more times and constructively interfere with other great-circulating Rayleigh waves. Such constructive interference can only occur for a strong source; this implies there are many weaker sources responsible for this portion of the spectra. The lack of constructive interference among many minor-arc arrivals can produce a broad peak like the one in Fig. 5 (top).

The hum was initially discovered as the background oscillations of the Earth around the year 1998 (Nawa et al. 1998; Suda et al. 1998; Kobayashi and Nishida 1998; Tanimoto et al. 1998; Kanamori 1998). It was recognized then that there were small oscillations that exactly matched the frequencies of fundamental spheroidal modes (Fig. 5, bottom), even in the absence of earthquakes with a moment magnitude of about 5.5. The amplitudes for these oscillations were shown to be equivalent to earthquakes with a moment magnitude of about 6 (Tanimoto and Um 1999) despite the fact there was no occurrence of such earthquakes. This discovery was about 100 years later than the discovery of the microseisms because their amplitudes were much smaller. Furthermore, the frequency band of the hum required high-quality broadband sensors that are sensitive at about 0.01 Hz.

Using the fact that spheroidal fundamental modes are equivalent to traveling great-circling Rayleigh waves, Ekström (2001) showed that there existed background great-circling Rayleigh waves in vertical component seismograms through the autocorrelation approach. This work also detected a large six-month periodicity in amplitudes that agreed with the modal study by Tanimoto and Um (1999). The maximum amplitudes were found in January and July. Ekström (2001) also reported that the amplitudes of the hum were equivalent to an earthquake of about magnitude 5.8 which was a more precise estimate than Tanimoto and Um (1999). Detection of seasonality finally made it clear that the cause of excitation was not of tectonic origin such as small earthquakes or slow slips on faults; the cause must be in the atmosphere or the oceans. This was reviewed in Tanimoto (2001) but a more recent, up-to-date review of the hum can be found in Nishida (2013).

2.3.2 Excitation mechanism

The initial hypothesis for the cause of the hum was the atmospheric excitation or pressure changes on Earth's surface. Random pressure changes on Earth's surface were assumed to excite the resonant vibration modes of the Earth (Kobayashi and Nishida 1998; Tanimoto and Um 1999; Fukao et al. 2002; Nishida et al. 2002). For such randomly distributed surface forces to excite normal modes, the crucial parameter turned out to be the lateral correlation length of surface pressure (Kobayashi and Nishida 1998). In hindsight, this hypothesis was untenable because the required correlation length of pressure to explain the observed modal amplitudes was 1–10 km. Such a long correlation length is incompatible with pressure observations. The observed pressure correlation length varies temporarily and spatially but is in the 10–100 m range most of the time.

Intuitively, the choice of ocean waves as the cause of excitation seems far more reasonable than the atmospheric hypothesis. This is because pressure perturbations

in the oceans are much larger than pressure perturbations in the atmosphere; for example, the largest pressure changes in the atmosphere occur when tropical cyclones develop but the pressure difference between the lowest pressure at their center (~900 hPa) and the average pressure outside (~1000 hPa) is at most 10% (100 hPa). In the oceans, ocean waves with amplitudes of about 10 m can be found quite commonly in winter of the northern hemisphere or the southern hemisphere. Pressure perturbations in such a situation can be as large as 1000 hPa, therefore the pressure perturbations could reach about 100%.

An oceanic excitation hypothesis was discussed earlier when the atmospheric excitation hypothesis was first proposed (Watada and Masters 2001), but it took a few years until the oceanic excitation hypothesis was seriously considered. In an observational study, Rhie and Romanowicz (2004, 2006) showed that the excitation sources of the hum were in the ocean by using broadband seismic arrays in Japan and California. This result suggested that ocean waves with frequencies of about 10 mHz were somehow generated (often called oceanic infragravity waves) and led to the excitation of solid Earth modes. Tanimoto (2005) also presented various supporting evidence for the oceanic excitation hypothesis from the analysis of seismic data from the IRIS global network data and the satellite significant-wave-height data (SWH). Specifically, the SWH data showed high-amplitude ocean-wave activities in January and July that matched the seasonal, maximum amplitudes of the hum. Further studies that improved the locations of the excitation sources and understanding of the excitation mechanisms were published by Nishida and Fukao (2007), Bromirski and Gerstoft (2009), Fukao et al. (2010), and Harmon et al. (2012). In general, the excitation sources in the oceans were found close to the coasts but were spatially spread out (Bromirski and Gerstoft 2009; Traer et al. 2012; Nishida 2017).

In theory, the hum could be excited in deep oceans because the long-period oceanic infragravity waves that are the cause of excitation have amplitudes that reach the ocean floor even in the open oceans (3–4 km). Examples of the eigenfunctions of ocean waves for the frequency band of the hum, about 10 mHz, are shown to reach the ocean bottom (Fig. 6). This is the case for the Preliminary Reference Earth Model (Dziewonski and Anderson 1981) which has an ocean depth of 3 km. The eigenfunctions only marginally reach the seafloor at 20 mHz (Fig. 6, right) but they have significant amplitudes on the seafloor at 10 mHz. These features in eigenfunctions suggest that the hum at 10 mHz may be excited by the direct interactions between ocean waves and the solid Earth in the open ocean, although the hum at 20 mHz can only be excited in shallower ocean areas. Therefore, in theory, the excitation of the hum could occur anywhere in the oceans (Tanimoto 2005). However, observational studies for the excitation sources of the hum seem to indicate the potential source areas are close to the coasts (Bromirski and Gerstoft 2009; Ermert et al. 2017; Harmon et al.

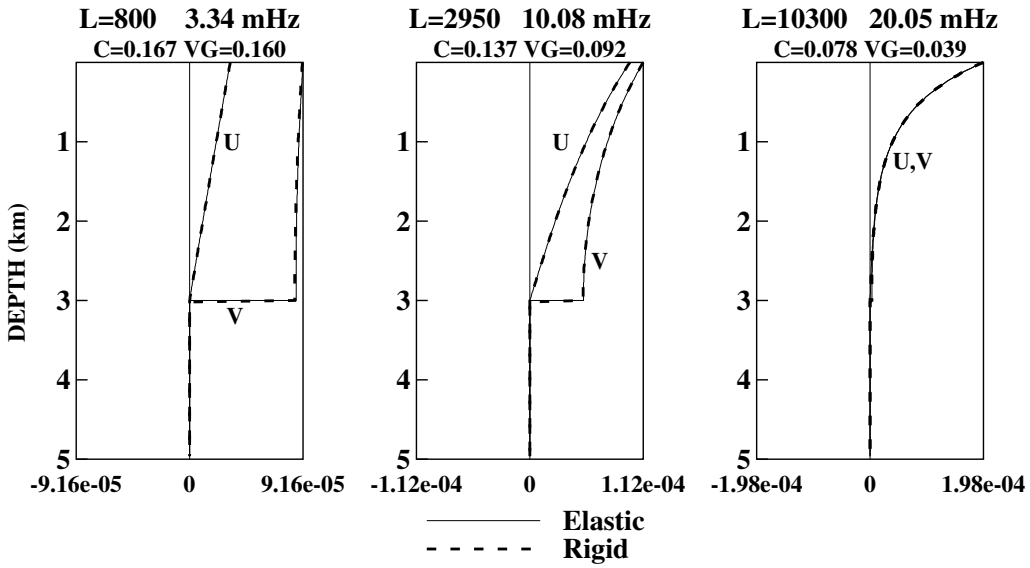

Fig. 6 Eigenfunctions of ocean-wave modes for PREM. U is the vertical function and V is the horizontal function of modes. At 0.02 Hz (20.05 mHz), U and V are equal, showing the typical circular particle motion of ocean gravity waves. At 0.003 Hz (left) and 0.010 Hz (middle), they have non-zero values at the ocean bottom. Any topographic deviation from a layered medium can cause scattering and generate Rayleigh waves at the same frequencies. Solid lines are for PREM (elastic model) and dashed lines are for the rigid ocean bottom model

2012). It is generally thought that the generation of low-frequency ocean infragravity waves preferentially occur in shallow oceans close to the coasts but we still do not have a clear understanding of this process (Ardhuin et al. 2014; Aucan and Ardhuin 2013; Dolenc et al. 2008; Herbers et al. 1995; Uchiyama and McWilliams 2008; Rawat et al. 2014).

Based on these developments, the cause of the hum is now generally considered to be in the ocean. However, there may be an exception at low frequencies, especially below 5 mHz (Nishida 2017). First of all, even though we stated that the low-frequency end of the hum is 3 mHz, the background noise, caused by atmospheric processes, increases toward lower frequency (Fig. 1) and precludes its definitive determination. This feature may be masking the background oscillation signals (Fig. 5) and if so, the lower frequency limit of 3 mHz is not certain. We note that Nawa et al. (1998) reported very low-frequency modes in their analysis for the background oscillations (hum). Although it seems to be the only paper to show such results, if their observations were true, the atmospheric process seems to be a serious candidate for the excitation of such a low-frequency part of the hum, because there is much more background energy in the atmosphere than in the oceans at low frequencies.

2.4 A unified view for the excitation of the microseisms and the hum

Ardhuin et al. (2015) claimed, following Hasselmann (1963), that there are two types of seismic-noise excitation by ocean waves. One is by the direct interaction between ocean waves and the solid Earth and the other is by the wave–wave interaction among ocean waves. The hum and the primary microseism are examples of the direct interaction and the secondary microseism is an example of the wave–wave interaction. Similar arguments were essentially made by Nishida and Fukao (2007), Nishida et al. (2008), Fukao et al. (2010), and Saito (2010). They also discussed the excitation mechanism of Love waves in the hum, caused by the interactions between propagating oceanic infragravity waves and the solid Earth through the ocean-floor topography. Both the excitation of Rayleigh and Love waves may be explained by this process.

An alternative excitation mechanism for the hum similar to the wave–wave interaction was proposed by Webb (2008) and was also analyzed by Tanimoto (2010). The reason that this process was proposed was that the excitation due to a collision of low-frequency ocean waves could become large for frequencies below 5 mHz. At such low frequencies, horizontal components of ocean-wave eigenfunctions become like that of Tsunami waves (modes) and have large amplitudes from the surface to the ocean floor. But this mechanism should create at least two spectral peaks, one corresponding to the frequency of ocean waves and the other being its double-frequency peak, as this process is a low-frequency version of the wave–wave interaction. Such a double-frequency feature has not been identified in observed data for the hum. It appears that the direct interaction is a better mechanism to explain the excitation of the hum, especially because it can also explain the excitation of Love waves that have been observed (Kurrle and Widmer-Schnidrig 2008).

3 Classification of seismic noise

We propose to classify seismic noise, first broadly by two types: (1) the propagating seismic noise and (2) the quasi-static deformation. The former type typically occurs due to sources at remote sites that emit seismic waves. Seismic noise consists of propagating body and surface waves of this type. The latter type is typically caused by large pressure variations near an observing station; pressure changes work as a load on the solid Earth and deform it almost statically at low frequency, even though pressure may vary with time.

For the first type, the propagating seismic waves, we will introduce an additional distinction between the oceanic sources and the on-land sources because we find many different processes in this type. The number of cases for quasi-static deformation is limited, and hence we will treat it as one category. This leads us to consider three different categories: (a) propagating seismic signals from sources in the ocean, (b) propagating seismic waves from on-land sources, and (c) the quasi-static deformation in the ocean (at sea bottom) or on land.

In our classification, the three main types of seismic noise, namely the primary microseism, the secondary microseism, and the hum are in the first category: (a) propagating seismic waves from ocean sources. We regard the distinction between the direct interaction and the wave–wave interaction as the next level of classification within this category.

In this paper, we stress the last category, the quasi-static deformation due to pressure loading effects. This is because, in recent literature, this type of seismic noise is not emphasized or sometimes ignored entirely. But recent observations with co-located pressure and seismic sensors have unequivocally shown that surface pressure can become the dominant cause of deformation for a short-term interval and it causes a quasi-static deformation of the medium by surface pressure loading. Such time intervals last from a few hours to days. For on-land seismic stations, it occurs when a strong wind blows over a station or high-amplitude atmospheric pressure waves, such as Lamb waves from the Hunga-Tonga eruption (Anthony et al. 2022), pass over a station. For stations

on the ocean floor, it occurs when oceanic infragravity waves pass over a station on the seafloor (Crawford et al. 1991; Webb and Crawford 1999) or when the ocean currents at the sea bottom change the sea-bottom pressure significantly. In all cases, the time interval of quasi-static deformation can be identified by monitoring the coherence between pressure and seismic data because coherence should become high when pressure loading is the cause of the deformation. At the same time, there should be little seismic-wave excitation during this deformation process.

4 Transient phenomena

As we stated earlier if we created seismic-noise spectra by averaging one-month-long time series, the results would be dominated by the three main types of noise: the primary microseism, the secondary microseism, and the hum (Fig. 1). But for a short-term interval from about a few hours to a week, we can see signals from other phenomena. Some phenomena simply show larger signals either in the time domain or in the spectral domain but others require a technique of signal stacking such as the beamforming method. In the latter case, raw amplitudes may be smaller than the background noise but a stacking approach makes it possible to identify the signals.

We will discuss such transient phenomena in this section. Specifically, we discuss (1) teleseismic body waves from tropical cyclones (TC), (2) stormquakes, (3) weather bombs, (4) higher-frequency noise in the frequency range 0.3–2 Hz due to local wind-generated ocean waves, (5) tornadoes, (6) tropical cyclones on land (after the landfall), and (7) the quasi-static deformations due to pressure loading. We will discuss them according to our classification scheme: (1) propagating seismic waves from oceanic sources (1, 2, 3, 4, in Sect. 4.1), (2) propagating seismic waves from on-land sources (5, 6, Sect. 4.2), and (3) quasi-static deformations in the ocean and on land (7, Sect.4.3).

4.1 Propagating seismic waves from oceanic sources

We discuss four phenomena from (1) to (4) in the above list. They all have excitation sources in the ocean but the detailed locations are quite different. Signals from a TC are typically from an open, deep ocean. Stormquakes are excited in a continental shelf, therefore close to the coast in general. Weather bombs also tend to be located close to the coast. The sources for higher-frequency noise between 0.3 and 2 Hz have been found in the open ocean as well as in coastal regions.

4.1.1 Teleseismic body waves from tropical cyclones (TC)

By using a network of about 150 broadband stations in Southern California, Gerstoft et al. (2006, 2008) and Zhang et al. (2010) demonstrated that teleseismic P-wave signals from a tropical cyclone (TC hereafter) can be identified by the beamforming analysis. Gerstoft et al. (2006) analyzed signals from Hurricane Katrina when its landfall occurred near New Orleans. Zhang et al. (2010) analyzed signals from Super Typhoon Ioke in 2006. The two results were some of the best early, clean demonstrations of P wave signals associated with TCs.

As the Ioke moved northward in the western Pacific Ocean (Zhang et al. 2010), the P-wave source could be identified in the neighborhood of its center and it moved with this TC. It was clear, however, that the P-wave beam (the excitation source) was not at or near the center of this TC but was shifted south by a distance of about 500–1000 km. It was as though the P-wave source was tracking the center of Ioke with this separation distance as the TC moved northward. Later studies by others confirmed the movement of the source. Those later studies included additional quantitative modeling of P-wave amplitudes, for example, by Farra et al. (2016) and Retailleau and Gualtieri (2021).

A similar spatial shift of the P-wave source from the center of a TC was also recognized for other hurricanes. An example from Hurricane Sandy in 2012 is shown in Fig. 7. This TC moved northward from the Caribbean Sea, off the East Coast of the USA. The P-wave source was also derived from the Southern California Broadband Network. In this case, the P-wave source was geographically shifted to the east of this hurricane. The source was not tracking behind the hurricane like the case for Ioke. Hurricane Sandy made landfall on the New Jersey coast and continued to move inland in the USA. The P-wave source in the ocean remained active for some time even after the landfall of Hurricane Sandy. This delayed phenomenon can be explained by the fact that P waves were generated by the wave–wave interactions in the ocean. There may also be an effect due to a slower response of the ocean-wave spectrum to changes in wind speed (Young 1999).

In general, seismic wave excitation associated with a TC while it is in the ocean is difficult to understand because of the complexity of nonlinear energy transfer between the atmosphere and the ocean. What has been analyzed theoretically so far, including the famous Longuet-Higgins (1950) formula, are only the first-order effects of the nonlinear advection term in the Navier–Stokes equation. When the wind blows hard and its strength is maintained for a long period, there should be more complex nonlinear effects emerge. If the nonlinear effects become severe, they will mix processes from different frequencies, making its understanding extremely difficult (e.g., Janssen 2004).

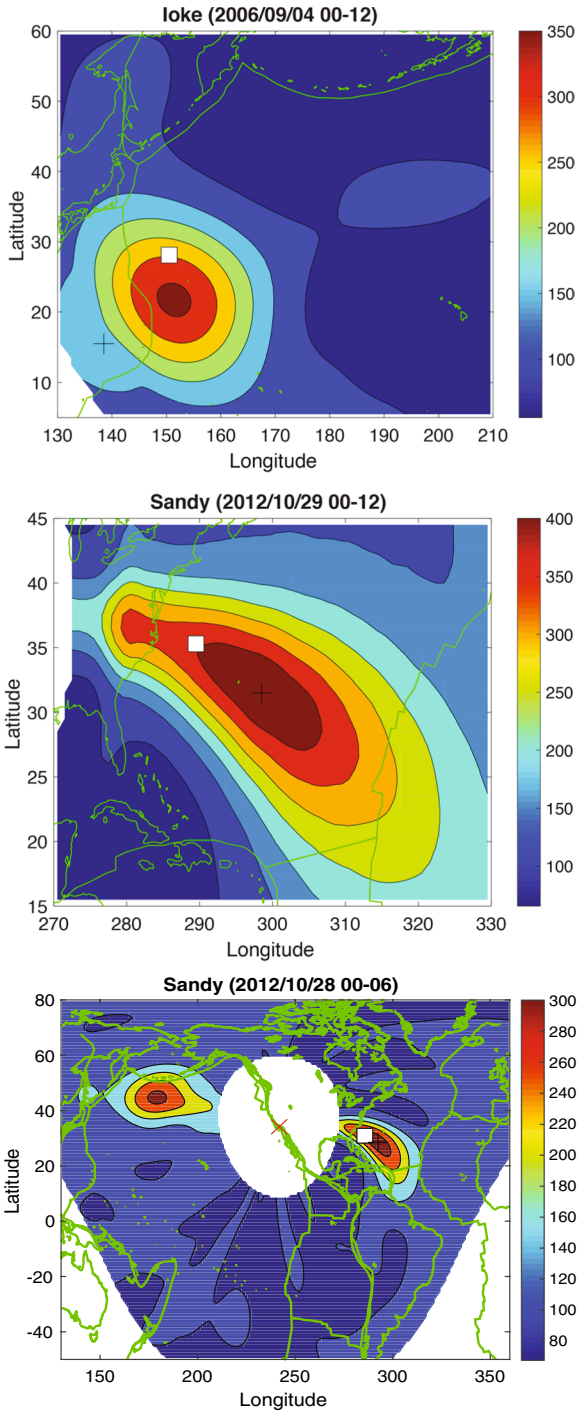

Fig. 7 Beamforming results for P-wave signals using the broadband seismic stations in Southern California with about 150 stations. (top) The beam for the P-wave source is tracking the center of Hurricane Ioke (white square box). (middle) The P-wave beam (dark red) is on the east side of the center of Hurricane Sandy in 2012 (white square box). (bottom) When Sandy was moving north off the east coast of the USA, there was also an independent P-wave signal from a low-pressure system (storm) in the northern Pacific Ocean. They typically create signals between about 0.15 Hz and 0.25 Hz, in the frequency band of the secondary microseism

4.1.2 Stormquakes

Fan et al. (2019) showed that during a large storm or a large TC, the interactions of long-period ocean waves with the solid Earth occur in shallow oceans, offshore of North America. This interaction was shown to excite Rayleigh waves in the 0.02–0.05 Hz range by analyzing seismic data from the EarthScope TA stations. These excitation sources were located in specific regions of the shallow ocean and had an equivalent magnitude of 3.5 or more in terms of their strength of excitation. These events were individually small but occurred over a large region off the coasts and were termed "stormquakes".

Stormquakes are likely generated by the direct interaction between ocean waves and the solid Earth. This is because the excited seismic waves were typically Rayleigh waves between 0.02 and 0.05 Hz whose eigenfunctions reach the upper mantle, well beyond the ocean bottom. Secondly, the spatial pattern of stormquakes suggested that a specific seafloor topography is required for their excitation. For example, one of the requirements seems to be an existence of a large continental shelf. Therefore, the direct interaction between ocean waves and the solid Earth within a large continental shelf seems to be required for the excitation.

Seismic signals from these sources may be used for a structural study, although the drawback is the requirement for a dense array like the EarthScope TA to locate the excitation sources. But such detection of stormquakes may become more common, as deployments of arrays with higher density arrays are happening in the world, such as AlpArray (Hetényi et al. 2018) and Hi-net (Obara 2003).

4.1.3 Weather bomb

Nishida and Takagi (2016) showed that a rapidly growing low-pressure system, a weather bomb off the coast of Greenland, generated body waves that were detected in Japan. The Hi-Net data consisting of about 600 stations in Japan (Obara 2003; Okada et al. 2004) were used to detect seismic signals from this "weather bomb". Their results showed that in addition to P waves, both SV waves and SH waves were identified by the beamforming analysis. The weather bomb is defined to be a low-pressure system whose pressure is rapidly dropping 1 (hPa/h) for 24 h. It is a rare and extreme event (Gerstoft and Bromirski 2016) but when it occurs, it can be an efficient source for seismic body waves that may be observed at distant seismic stations (70–90 deg).

A similar excitation of P waves can be recognized even for a weaker low-pressure system. In Fig. 7, P-wave sources for Super-typhoon Ioke (Fig. 7a) and Hurricane Sandy (Fig. 7b) are shown. When Sandy approached the

New Jersey coast, the array in Southern California also detected a low-pressure system in the opposite direction in the Northern Pacific Ocean (Fig. 7c). This low-pressure system was not reported, presumably because it was in a remote area in the deep ocean and posed no risk to human society. But clearly, it is possible to detect P-wave energy from such a low-pressure system, using an ordinary beamforming method. This type of low-pressure system may be quite common.

4.1.4 *Higher frequency noise 0.3–2 Hz due to local wind-ocean waves*

Figure 8 shows that seismic spectra (PSD) (top panel), ocean wave spectra (second panel), wind speed and direction data (third panel), all plotted against time

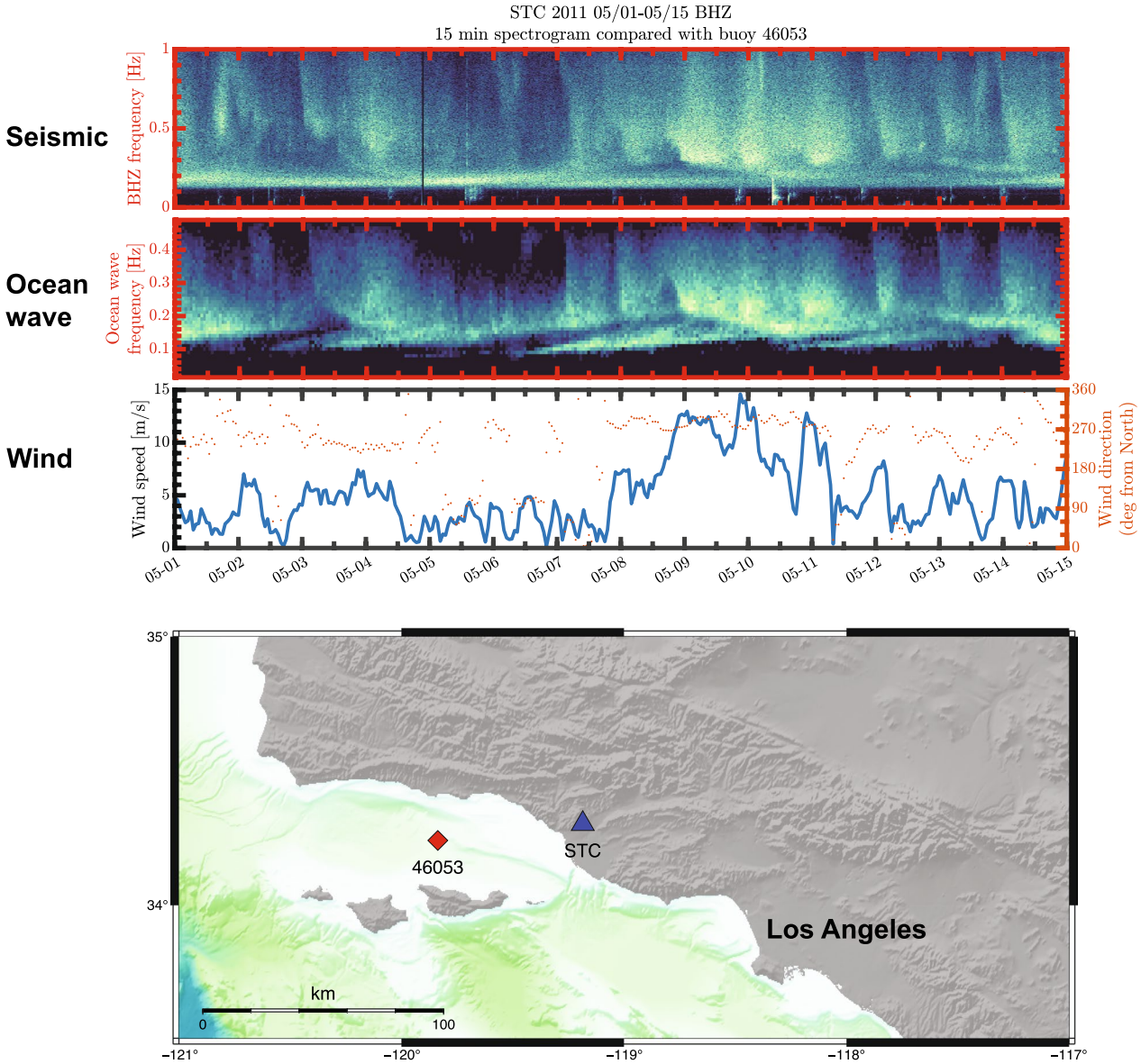

Fig. 8 (Top panel) Seismic data (PSD) from station STC in California (bottom panel) for two weeks from May 1 to May 15 in 2011. The frequency range (vertical axis) is from 0 to 1 Hz. White indicates high amplitude (PSD) and dark blue indicates low amplitude. (Second panel) Ocean wave spectra at buoy 46,053 **of** the same period (May 1–15). The frequency range (vertical) is from 0 to 0.5 Hz as this was the only available range. White indicates high amplitude and dark blue indicates small. (Third panel) Wind speed (blue line) and wind direction data at buoy 46,053. Wind direction (scale on right) is relatively constant at about 270 deg which means the westerly winds dominate most of the time. The scale for wind speeds is on the left (vertical axis). (Bottom panel) The locations of buoy 46,053 (red) and station STC (blue)

(horizontal axis), and a map that shows the locations of the buoy (45,053) and the seismic station STC (bottom panel). Ocean wave spectra and wind data were from buoy 46,053 in the Santa Barbara strait (Fig. 8, bottom) and seismic data were from STC, therefore the location of seismic data is close to the location of ocean-wave and wind data but not the same. The horizontal axis is the day from May 1st to 15th in 2011 for the three top panels.

In seismic and ocean-wave data, amplitudes are indicated by color in decreasing order from white (high) to dark blue (low). The whiter the color, the higher the amplitudes. In the ocean-wave panel, there are multiple signals for frequencies below about 0.2 Hz that are oblique and parallel. This trend of oblique patterns shows that the lower-frequency signals arrive earlier than the higher-frequency signal and the whole dispersive wave train last about 4 days. There are four such wave trains in Fig. 8 (ocean wave panel) during the 15-day time interval. This oblique pattern indicates that these signals are the arrival of swells (ocean waves) generated by a distant storm; since ocean waves are dispersive and those at lower frequencies have higher propagation speeds, the lower frequency signals arrive first. Higher frequency signals follow in succession. These oblique trends are proof that they were generated at faraway locations. When these swell arrive at the coast, they generate the primary microseism and secondary microseism for frequencies below about 0.25–0.3 Hz.

But in the same figures, we note many vertically elongated white streaks span from about 0.3 Hz to 1.0 Hz, both in seismic and ocean-wave data. There are multiple examples of such features in white during this 15-day-long period. Comparison of these data with the wind speed data (blue line in the third panel, Fig. 8) shows that high amplitudes of seismic and ocean-wave data (white regions) generally agree with the time intervals of high wind speeds. When wind speed exceeded 10 (m/s) from about May 9th to 11th, there are three peaks in wind speed data and three distinct, corresponding white regions in both seismic and ocean-wave data, suggesting relationships among them. When wind speed goes down after May 11th, seismic signals generally become weak; Ocean waves also become less energetic, as indicated by dark blue areas.

These relationships imply that the seismic noise above 0.3 Hz is related to the local wind and its associated ocean wave behaviors. Even though seismic data in Fig. 8 stops at 1 Hz, similar patterns extend to higher frequencies up to about 2 Hz. The most natural explanation for their correlations seems to be that as wind becomes strong, wind-generated ocean waves are excited that in turn excite seismic signals. The part that connects ocean waves and seismic signals requires the wave–wave interaction because the ocean depth at the location of the buoy (46,053) is larger than the depth extent of ocean waves at frequencies 0.3–2.0 Hz.

Similar but independent evidence for wind-generated seismic noise was pointed out by Zhang et al. (2009, 2010) for regional data in Central California. Also, Bromirski et al. (2005) claimed, based on an ocean-bottom seismometer located at a halfway point between Hawaii and the continental USA and wind data in its neighborhood, that locally generated wind ocean waves are generating seismic noise in the same frequency band. A similar wind-generated seismic noise was also identified by an array study by Gal et al. (2015) and Pyle et al. (2015). In these studies, it was claimed that wind-generated ocean waves in an open ocean were generating similar high-frequency signals and body-wave signals were detectable through a careful analysis of multiple seismic arrays. The case of Zhang et al. (2010) is similar to our case in Fig. 8 as the source was close to the coast but the other three cases were in the open ocean.

These observations indicate that wind-generated ocean waves are creating seismic noise in the frequency band of about 0.3–2.0 Hz both in the open ocean and in the coastal region. This higher-frequency noise is distinct from the microseisms because the microseisms are mainly generated by ocean swells that are originally generated at distant locations by storms and propagate a long distance to the coasts.

4.2 Propagating seismic waves from on-land sources

For this category, we discuss two phenomena, (1) tornado and (2) tropical cyclone after the landfall. In both cases, propagating seismic waves are generated by sudden changes in surface pressure. In the case of tropical cyclone, there may also be some effects of pressure loading in addition to seismic wave generation but the data indicate that the loading effects alone cannot explain the data.

4.2.1 Tornado

Tornados are mostly atmospheric phenomena and their monitoring and forecasting are done using data from surface weather stations and the incoherent scatter and Doppler radars (Mitchell et al. 1998). These approaches can detect a possible location of tornado and funnel clouds but determining the timing of a tornado touchdown still relies on storm chasers and spotters. Alternative detection methods have been pursued by studying seismic and infrasound signals (Talmadge and Waxler 2016; Tatom et al. 1995; Tatom and Vitton 2001) but the analysis tended to be focused at frequencies above 1 Hz.

Valovcin and Tanimoto (2017) investigated seismic signals for frequencies between 0.01 and 0.03 Hz for the

touchdown of tornado Joplin in 2011. Joplin was a significant tornado with an Enhanced Fujita Scale 5 (EF5, http://www.spc.noaa.gov/efscale/) which exhibited wind gusts over 200 mph (about 90 m/s). Seismic signals were detected clearly at station T38A, an EarthScope TA station about 2 km from the tornado track, but other EarthScope stations, more than about 70 km away from the tornado track, did not show clear seismic signals. Figure 9 (top) illustrates the arrival of airwaves (infrasound) and seismic waves from a tornado touchdown and Fig. 9 (bottom) shows an inverted surface pressure source as a function of time. The source of seismic waves was assumed to be a vertical force that ran along the tornado touchdown track. For vertical data, this is a reasonable assumption as the pressure inside a tornado is very low due to high-speed winds and most tornado damages include things that fly away from the Earth's surface. Although the swirling motion of the winds was not modeled in this study, this approach may be justified for the analysis of vertical component seismic data.

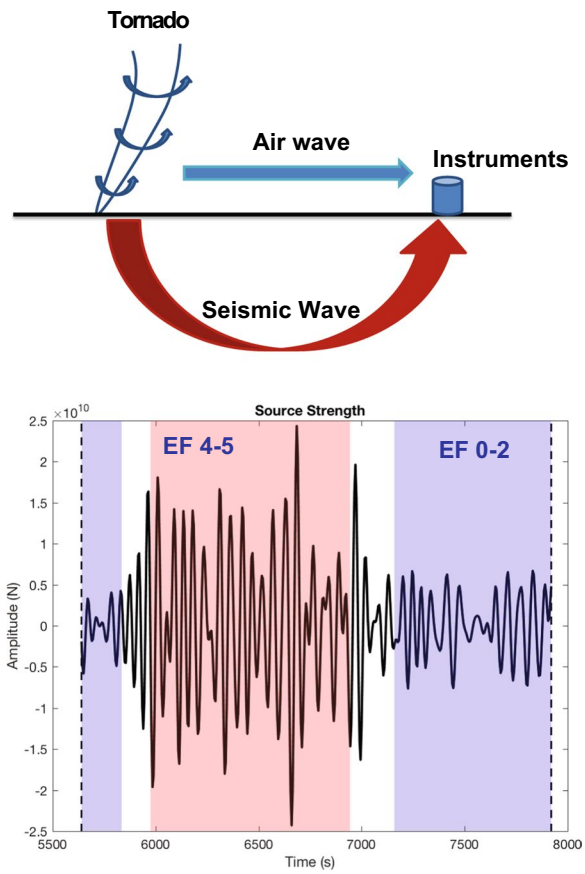

Fig. 9 (top) Tornadoes generate airwaves and seismic waves. Seismic waves primarily come when a tornado touches the ground. Because the pressure in the interior of a tornado is low (due to fast wind speeds), things get sucked upward. (Bottom) The pressure source along the tornado track was inverted and shown as a time series. When the tornado was strong (EF4–5), the pressure source was strong, and when it became weaker (EF0–2), the pressure source became weak. Seismic data may be used for quantitative analysis of the effects of tornadoes

The time series for the inverted source strength in Fig. 9 (bottom) shows that the source strength (surface vertical forcing due to pressure) correlates with the EF scale; note that when the EF scale was about 4–5, the vertical force had large amplitudes and when the EF scale became low about 0–2, the inverted source strength was much weaker. Therefore, by analyzing seismic data, we can estimate the violent effects of a tornado touchdown.

However, the use of seismic data for this purpose may be hard in practice. This is because even this significant tornado did not create large seismic signals at adjacent stations in the EarthScope Network, the closest stations being typically 70 km away. Only the data at a distance of 2 km from the track showed analyzable signals. This rapid decay with distance seems to indicate that this approach of using low-frequency seismic signals is not viable for tornado monitoring, as it would require a much higher-density network. It seems more promising to analyze seismic signals from a higher frequency range or infrasound data for monitoring tornadoes.

4.3 Tropical cyclones on land

A TC (hurricane or typhoon) becomes strong when it travels over a warm ocean (above 26 °C) because of the energy supply from the ocean below through the latent heat (Emanuel 1986, 1991). But after the landfall, a TC decays quickly because there is no more supply of energy from the land below. Tanimoto and Lamontagne (2014) and Tanimoto and Valovcin (2015) showed that seismic and pressure data at low frequency (0.01–0.02 Hz) from the EarthScope TA stations can be used to monitor how a TC decays. Right after the landfall of Hurricane Isaac in 2012, this hurricane went through the TA stations which were equipped with seismic as well as pressure sensors. Both seismic and pressure data showed the maximum peak at the location of the circular eyewall, a distance about 80–100 km from the center. Figure 10 shows seismic data in the left panels and pressure data in the right panels. The top panels show seismic and pressure amplitudes on maps and the bottom panels show amplitudes plotted against the distance from the center of this TC. Colors are used to indicate three different levels of amplitudes (Power Spectral Density). In both data, the peaks are found at about 80–100 km and the amplitudes decay outward up to about 600–800 km. It seems reasonable to interpret the location of the maximum amplitudes as the eyewall. Inside the eyewall, seismic and pressure amplitudes

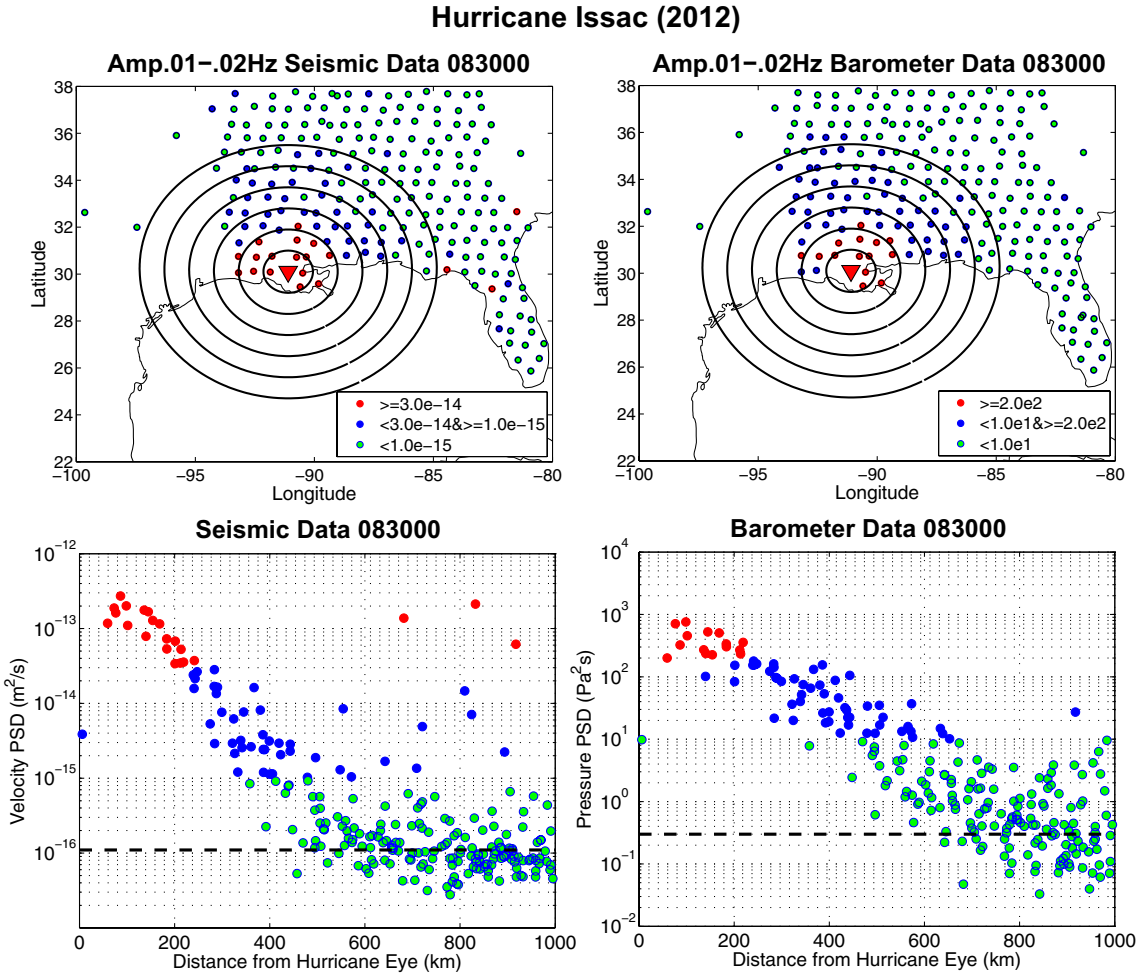

Fig. 10 (Top-Left) Seismic amplitudes (PSD averaged between 0.01 and 0.02 Hz) from Hurricane Isaac on a map. (Bottom-Left) The same amplitude results are plotted as a function of distance from the Hurricane center, indicated by a red triangle in the map. (Top-Right) Pressure amplitudes (PSD averaged between 0.01 and 0.02 Hz) on a map. (Bottom-Right) The same pressure amplitude results are plotted against the distance from the Hurricane Center. The peak amplitude distance is about 80–100 km from the Hurricane center and is likely to be the location of the eyewall of Hurricane Isaac. Amplitude decay is slightly different between seismic data and pressure data

were quite small although the number of stations within the eyewall was limited. The whole structure that surrounded the center of this TC decayed in about 3–4 days and could be monitored through seismic and pressure data.

For an on-land hurricane, pressure data are the cause of excitation and seismic data are the resulting disturbances. In Tanimoto and Valovcin (2015) the stochastic excitation theory was invoked to model these data. But there may be some effects from surface pressure loading in seismic data which was not incorporated in their analysis. However, the pressure loading alone cannot explain the data in Fig. 10, because the decay distance of seismic data (about 500–600 km) is different from that of pressure data (about 700–800 km). The loading effects alone, at least within the linear theory, should create the same pattern for seismic and pressure data. The differences in decaying patterns indicate the generation of propagating seismic waves that tend to make seismic amplitudes higher near the center of this TC.

4.4 Quasi-static deformation in seismic noise

The importance of quasi-static deformation has been recognized in at least two phenomena. The first case is the seafloor observation with co-located pressure and seismic instruments (Crawford et al. 1991; Webb et al. 1991; Webb and Crawford 1999). The second is the on-land observation with co-located pressure and seismic instruments (e.g., Sorrells 1971; Sorrells et al. 1971; Sorrells and Goforth 1973; Tanimoto and Wang 2018, 2019,

2020, 2021; Wang and Tanimoto 2020, 2022). We use the on-land case to describe the nature of this type of noise.

When atmospheric pressure changes slowly on the Earth's surface, the solid Earth deforms elastically by responding to surface pressure loading. If we have seismic and pressure sensors at the same location, we can monitor how the surface pressure is changing and how the solid Earth is responding to it. Two co-located sensors essentially show the source (pressure) and the response (seismic ground deformation). The data indicates that when surface pressure becomes large, the solid Earth deforms as if statically, responding to the loading pressure at each time instance. This process is more like a static deformation and hardly generates propagating seismic waves.

An example from a co-located pair of seismic and pressure sensors from an EarthScope TA station U57A is shown in Fig. 11. Figure 11a shows the vertical seismic amplitudes (PSD) plotted against the pressure amplitudes (PSD). Each point represents pressure and seismic PSD from one-hour-long time series and the whole plot was derived from the entire year of 2014. Red points indicate the time intervals of high coherence (> 0.7) between pressure and seismic data and blue points indicate time intervals of low coherence (< 0.7).

Figure 11a shows that when pressure is low, vertical seismic amplitudes are nearly constant. But if pressure exceeds a certain threshold value, in this case about 1 (Pa^2/Hz), vertical amplitudes change with pressure amplitudes. This trend suggests that the local pressure is controlling the amplitudes of seismic noise for pressures above a certain pressure threshold.

Red circles in Fig. 11a (high coherence time intervals) appear mostly when the pressure is higher than a threshold value. High coherence indicates that the waveforms are similar. This distribution of high-coherence time intervals also supports that the pressure (source) and seismic data (resultant deformation) are under a causal relationship.

Figure 11b shows a plot between the wind speed PSD and the vertical seismic PSD. The pressure PSD in Fig. 11a was replaced by the wind PSD data. There are large scatters in this plot but we can see that the basic structure of the relationship is similar to Fig. 11a; when the wind speed PSD is low, the vertical seismic amplitude is nearly constant but beyond a threshold wind speed, the vertical seismic amplitudes and the wind speed PSD go up and down in tandem. This is because variations in wind speed are the main cause of surface pressure changes. If the wind speed is v and atmospheric density is ρ, pressure changes approximately as $(1/2)\rho v^2$. Figure 11b illustrates this at 0.02 Hz but similar behaviors can be confirmed within the frequency range 0.01–0.05 Hz.

If we examine the phase relationship between pressure and vertical displacement, their phases are approximately 180° apart (Fig. 11d), meaning that when pressure becomes high, vertical displacement is negative or the surface is pushed downward. This relationship conclusively shows that the deformation is caused by the pressure-loading effect (Fig. 11e). This phenomenon was correctly analyzed and formulated by Sorrells (1971) for a homogeneous half-space in the early 1970s. It was later extended to a multi-layered medium (Sorrells and Goforth 1973). The method was taken up by Tanimoto and Wang (2018, 2019, 2020) to analyze the co-located pressure and seismic data from the EarthScope TA Network. Using this method, Vs30 for all the TA stations was estimated (Wang and Tanimoto 2020, 2022).

A similar situation was also noted for the seafloor observation of co-located pressure and seismic sensors (Crawford et al. 1991; Webb et al. 1991; Webb and Crawford 1999). In this case, highly coherent time intervals occurred when the ocean infragravity waves passed over a seafloor seismic station (Webb et al. 1991). The deformation is caused by pressure loading effects and is a case of quasi-static deformation, similar to the on-land cases. Using pressure and seismic data, the elasticity of shallow sedimentary layers can be determined by taking the ratio between pressure and seismic amplitudes. Following the phrase "Seafloor Compliance Method" by Crawford et al. (1991), this type of method of estimating near-surface (seafloor) elasticity is often called the compliance method.

5 Modern perspectives on two puzzles

5.1 Are the sources pelagic or coastal?

With the title "Microseisms: Coastal and Pelagic Sources", Haubrich and McCamy (1969) discussed that there is great uncertainty about the source locations of microseisms. The source of primary microseism was not an issue as the direct interaction between ocean waves and solid Earth can only occur in shallow oceans or near the coasts. The main argument arose because of the source locations of the secondary microseisms. They can be excited, in principle, in oceans of any depth by the wave–wave interactions (Longuet-Higgins 1950). This problem has remained a puzzle, although some have argued that both pelagic and coastal sources have to be considered (e.g., Chevrot et al. 2007; Landès et al. 2010). This question still became a contentious point of disagreement among some researchers (e.g., Kedar et al. 2008; Bromirski et al. 2013). But it appears that the research from the past decade has turned this question into a moot one, in essence strengthening the argument by Chevrot et al. (2007).

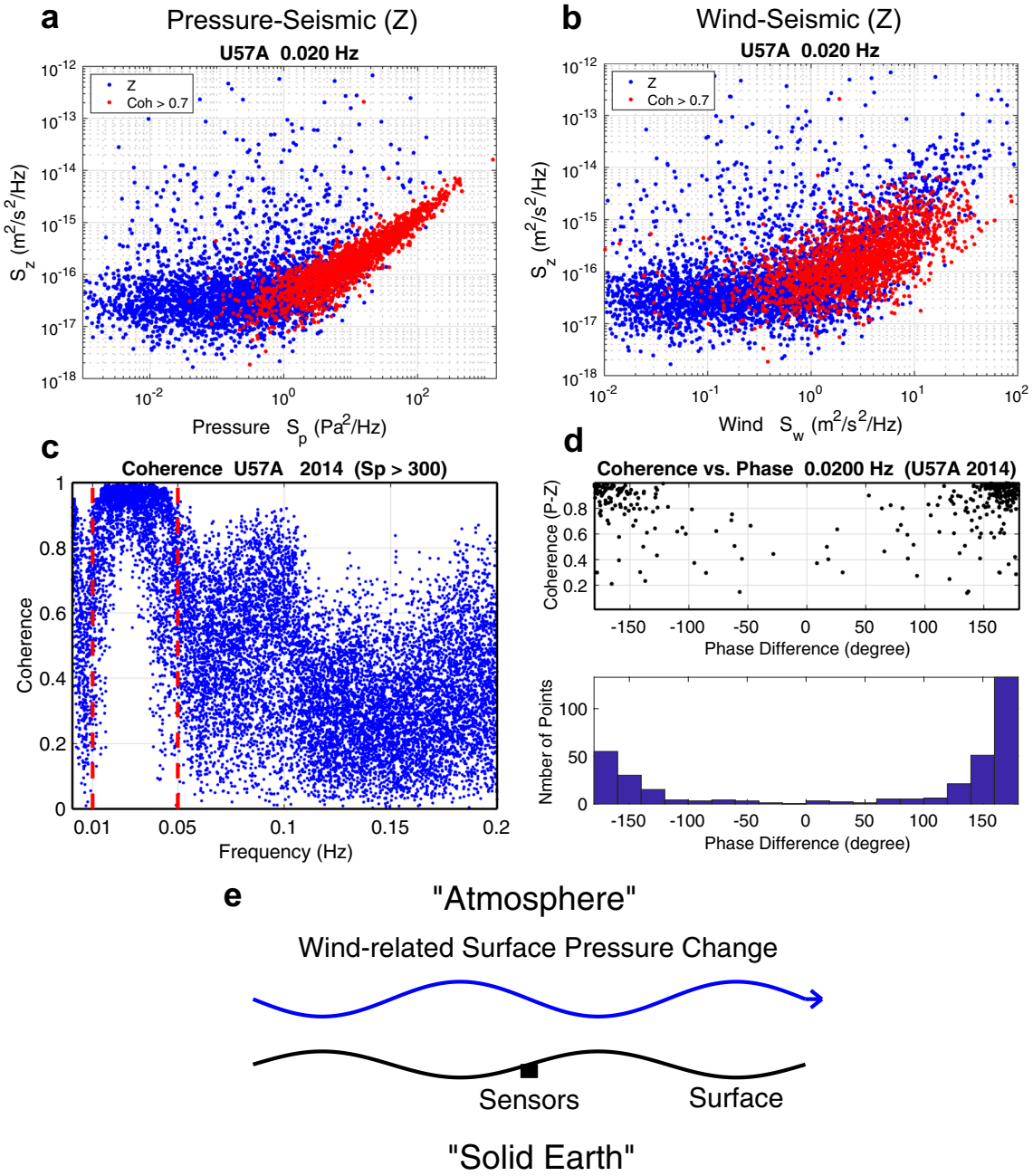

Fig. 11 **a** Co-located pressure vertical seismic data (both PSD, denoted by S_P and S_Z) are plotted for an EarthScope station U57A. Each point is from a one-hour time interval and data from the entire year of 2014 are plotted. Red indicates the time intervals when coherence between pressure and vertical seismic data was high (> 0.7). The threshold pressure is about 10^0 (Pa^2/Hz); above it, local pressure and seismic vertical amplitudes become correlated. Also, high-coherence time intervals are when pressure exceeds this threshold. **b** Co-located wind speed and vertical seismic data are plotted. The vertical scale is the same as **a**. Pressure data in **a** were replaced by wind speed data. The vertical axis The overall similarity to **a** indicates that surface pressure is closely related to wind. **c** Frequency dependence of coherence for time intervals with pressure PSD higher than 300 (Pa^2/Hz). There is a high-coherence frequency interval of approximately 0.01 Hz to 0.05 Hz, indicated by red vertical dashes. **d** Phase difference between pressure and vertical displacement. When pressure is high, the phase differences are about 180° (opposite phase). **e** An illustration of the relationship between pressure and vertical displacement. When pressure is high, the ground surface gets pushed down and vice versa. This is the manifestation of the quasi-static deformation

This question has been answered mainly due to the feasibility of mapping the locations of wave–wave interactions by beamforming analysis of dense array data. Array analysis of surface waves (Toksöz and Lacoss 1968; Cessaro and Chan 1989; Cessaro 1994; Friedrich et al. 1998; Gerstoft and Tanimoto 2007) have provided useful results before but the new developments are mainly for body waves which require a much denser distribution of seismic stations. By focusing on body waves, especially P waves (Neale et al. 2017, 2018; Reading et al. 2014; Xiao et al. 2021), it is now possible to map the locations and the strength of equivalent forces on a global scale (Nishida and Takagi 2022). Even the seasonal variations are detectable through the variations in the strength of sources. The results show the global distribution of excitation sources for the secondary microseism.

But this does not mean that the signals in observed secondary microseism are dominated by the global, pelagic sources. While a seismic array can pick up signals from far away, the dominant signals may be from a near coastal region. For example, an observation at a California station is more likely to be dominated by sources near the coast. There are two reasons for this. First, the wave–wave interactions occur quite commonly near the coast because of the reflection of ocean waves from the coast. The second reason is related to the nature of surface waves that are generated by the wave–wave interaction. Because the excitation source is shallow, the amplitudes of surface waves (mostly Rayleigh waves) tend to dominate body wave signals. For this reason, seismic noise in the frequency band of secondary microseisms at coastal stations shows large signals from surface waves (Tanimoto et al. 2006). But there is also another reason that observed surface waves in the secondary microseism tend to be from nearby sources. It is related to the nature of surface waves at about 0.15 Hz. At this frequency, the wavelength and the depth extent of surface waves are not large. When surface waves, generated in deep (pelagic) oceans, arrive at the continental shelf region, their amplitude can suffer from scattering at the continental shelves (Bromirski et al. 2013). This would cause reflection of some portion of energy as well as transmission, but the transmitted energy consists of scattered waves, consisting of body waves, and converted Love waves (Gualtieri et al. 2015, 2020). Therefore, the observed secondary microseisms in coastal regions, such as California, are often dominated by surface waves generated from the nearby coastal region. But if we analyzed seismic array data for the same time interval, we expect to detect body waves from teleseismic sources caused by the wave–wave interactions (Nishida and Takagi 2016, 2022; Liu et al. 2016; Xiao et al. 2021).

In summary, it seems safe to state that the wave–wave interactions are occurring globally all the time. But the signals in the frequency band of secondary microseism at a particular location may be dominated by nearby sources, especially by surface waves excited by them.

5.2 Love wave excitation in the secondary microseisms

It is not surprising to find SH-type body waves or Love waves in the primary microseism. As ocean waves approach the coastal area and interact with the solid Earth through the topography in shallow oceans, this interaction can produce an equivalent horizontal force (e.g., Saito 2010). But it is surprising to see Love waves in the secondary microseism because the equivalent force to the wave–wave interaction is primarily vertical. The mechanism of wave–wave interaction does have a coupled horizontal force due to a collision of ocean waves (Tanimoto 2010) but its effects are very small at 0.15 Hz.

Observationally, the existence of Love waves in the frequency band of secondary microseism has been clear for a long time. But the quantitative estimate of their ratio relative to the amount of Rayleigh waves became reliable only recently (Matsuzawa et al. 2012; Juretzek and Hadziioannou 2016; Tanimoto et al. 2015a, b, 2016a, b; Le Pape et al. 2021). Those results indicated that the ratio of Love-wave energy to Rayleigh-wave energy varied widely from 10 to 100% at different locations (100% means comparable to Rayleigh waves). The ratios also varied seasonally at each location.

The origin of such Love waves may be explained by two mechanisms; one is the action of vertical force (wave–wave interaction) on seafloor topography or a slope that contains deviation from a layered structure. The other is through the conversion from Rayleigh waves to Love waves as they propagate from the source to an on-land seismic station. Gualtieri et al. (2020) used a numerical simulation method for a realistic 3D structure and demonstrated that conversion from Rayleigh waves to Love waves can occur and can explain the observed Love wave amplitudes. A serious conversion effect was also discussed by Bromirski et al. (2013), although they primarily stressed a reduction of fundamental Rayleigh wave energy when Rayleigh waves propagate through the ocean-continent transition region. It appears that the second mechanism, a conversion during wave propagation from an ocean to a continent, seems to be a more viable process for generating Love waves.

6 Summary and discussion

We reviewed seismic noise in the frequency band from about 0.003 Hz to 1 Hz. In addition to the three main seismic noises, namely (1) the primary microseism (0.05–0.07 Hz), (2) the secondary microseism (0.1–0.4 Hz), (3)

the hum (0.003–0.015 Hz), there are transient, short-term noise-generating phenomena that last from a few hours to a week in this frequency band. Seven examples were discussed: tropical cyclones (Hurricanes and typhoons) in the ocean, stormquakes, weather bombs, higher frequency seismic noise between about 0.03 and 2 Hz that are generated by locally-generated ocean waves, tornadoes, on-land tropical cyclones (after landfall), and pressure loading that cause quasi-static deformations.

Table 1 summarizes our classification scheme of seismic noise. We propose to classify seismic noise broadly by three categories, (a) propagating seismic waves from oceanic sources, (b) propagating seismic waves from on-land sources, and (c) pressure-loading quasi-static deformation on land and the seafloor. The three main seismic noises between 0.003 and 1.0 Hz are in (a). Since the primary microseism and the hum are generated by the direct interaction between ocean waves and the solid Earth (DI) and the secondary microseism by the wave–wave interactions among ocean waves (WW), we further divide this category into two sub-categories.

Seven different types of seismic noise, all emerging as temporary deviations from the three main seismic noises, are discussed in the text and are listed in Table 1. The dominant source is indicated by a circle for each case. The question mark is added for on-land tropical cyclones because there may be some significant loading effects in this case, even though seismic wave generation is indicated by seismic and pressure data.

We must end with a caution. Our understanding of seismic noise is making progress rapidly, especially our knowledge of the ocean processes. Soon, we will probably have an improved global map of source locations that are locations of the wave–wave interaction (e.g., Nishida and Takagi 2022), and their seasonal changes in the intensity of their forcings. Also, we will most likely discover new types of seismic noise from seafloor observations, particularly by the fiber-optic cable observations (e.g., Xiao et al 2022). Progress seems quite rapid and a new review will likely have to be written within the next 5 years.

Abbreviations

IRIS Incorporated Research Institutions for Seismology
SCEC Southern California Earthquake Center

Acknowledgements

This work was supported by the SCEC matching fund at UC Santa Barbara. TT gratefully acknowledges the support from the John Simon Guggenheim Foundation.

Author contributions

TT conceived and designed this review for low-frequency seismic noise. AA analyzed seismic, ocean-wave, and wind data for clarifying wind-generated seismic noise. Both authors read, edited, and approved the final manuscript.

Funding

This work was supported by the John Simon Guggenheim Fellowship and the SCEC (Grant Number 255732 (2022-2023)) matching fund at UC Santa Barbara.

Availability of data and materials

This review is based on published articles in various peer-reviewed journals in geophysics.

Declarations

Competing interests

The authors declare that they have no competing interests.

Table 1 Forcing mechanisms of various seismic noise in three categories

	Frequency range (Hz)	Category 1		Category 2	Category 3
		PSW ocean		PSW land	QS
		DI	WW		
Primary MS	0.05–0.07	O			
Secondary MS	0.1–0.3		O		
Hum	0.003–0.015	O			
TC in the Ocean	0.15–0.25		O		
Stormquakes	0.02–0.05	O			
Weather Bomb	0.01–0.02		O		
Wind ocean waves	0.3–2.0		O		
Tornado	0.01–0.03			O	
TC on Land	0.01–0.03			O	?
Pressure loading deformation on land and seafloor	0.01–0.05				O

Category 1 is Propagating Seismic Waves (PSW) from ocean sources. Category 2 is PSW from on-land sources and Category 3 is the quasi-static deformation (QS). Category 1 is divided into two cases, the Direct Interaction between ocean waves and solid Earth (DI) and the Wave–wave interaction among ocean waves (WW). MS is Microseism, and TC is Tropical Cyclone

Received: 25 April 2023 Accepted: 4 September 2023
Published online: 11 September 2023

References

Aki K, Richards PG (2002) Quantitative seismology, 2nd edn. University Science Books, Sausalito
Anthony R, Ringler A, Tanimoto T, Matoza R, De Angelis S, Wilson D (2022) Earth's upper crust seismically excited by infrasound from the 2022 Hunga Tonga-Hunga Ha'apai eruption, Tonga. Seismol Res Lett 20:1–14. https://doi.org/10.1785/0220220252
Ardhuin F, Gualtieri L, Stutzmann E (2015) How ocean waves rock the Earth: Two mechanisms explain microseisms with periods 3 to 300 s. Geophys Res Lett 42:765–772
Ardhuin F, Herbers THC (2013) Noise generation in the solid Earth, oceans, and atmosphere, from nonlinear interacting surface gravity waves in finite depth. J Fluid Mech 716:316–348
Ardhuin F, Rawat A, Aucan J (2014) A numerical model for free infragravity waves: Definition and validation at regional and global scales. Ocean Model 77:20–32
Ardhuin F, Stutzmann E, Schimmel M, Mangeney A (2011) Ocean wave sources of seismic noise. J Geophys Res 116:1–21
Aucan J, Ardhuin F (2013) Infragravity waves in the deep ocean: An upward revision. Geophys Res Lett 40:3435–3439
Beauduin R, Lognonné P, Montagner JP, Cacho S, Karczewski JF, Morand M (1996) The effects of the atmospheric pressure changes on seismic signals or how to improve the quality of a station. Bull Seismol Soc Am 86:1760–1769
Bernard P (1990) Historical sketch of microseisms from past to future. Phys Earth Planet Inter 63:145–150
Bromirski PD, Duennebier FK, Stephen RA (2005) Mid-ocean microseisms. Geochem Geophys Geosyst 6:Q04009
Bromirski P, Flick RE, Graham N (1999) Ocean wave height determined from inland seismometer data: Implications for investigating wave climate changes in the NE Pacific. J Geophys Res 104(C9):20753–20766
Bromirski PD, Gerstoft P (2009) Dominant source regions of the Earth's "hum" are coastal. Geophys Res Lett 36:L13303
Bromirski PD, Stephen RA, Gerstoft P (2013) Are deep-ocean-generated surface-wave microseisms observed on land? J Geophys Res 118:3610–3629
Cessaro R (1994) Sources of primary and secondary microseisms. Bull Seismol Soc Am 84:142–148
Cessaro RK, Chan WW (1989) Wide-angle triangulation array study of simultaneous primary microseism sources. J Geophys Res 94:15555–15563
Chevrot S, Sylvander M, Benahmed S, Ponsolles C, Lefèvre JM, Paradis D (2007) Source locations of secondary microseisms in Western Europe: evidence for both coastal and pelagic sources. J Geophys Res 112:1–19
Crawford W, Webb S, Hildebrand J (1991) Seafloor compliance observed by long period pressure and displacement measurements. J Geophys Res 96:16151–16160
Dahlen FA, Tromp J (1998) Theoretical global seismology. Princeton University Press, Princeton
Dolenc D, Romanowicz B, McGill P, Wilcock W (2008) Observations of infragravity waves at the ocean-bottom broadband seismic stations Endeavour (KEBB) and Explorer (KXBB). Geochem Geophys Geosyst 9:Q05007
Dziewonski A, Anderson DL (1981) Preliminary reference earth model. Phys Earth Planet Inter 25:297–356
Ekström G (2001) Time domain analysis of Earth's long-period background seismic radiation. J Geophys Res 106:26483–26493
Emanuel KA (1986) An air–sea interaction theory for tropical cyclones. Part i J Atmos Sci 43:585–604
Emanuel KA (1991) The theory of hurricanes. Annu Rev Fluid Mech 23:179–196
Ermert L, Sager K, Afanasiev M, Boehm C, Fichtner A (2017) Ambient seismic source inversion a heterogeneous Earth: Theory and application to the Earth's hum. J Geophys Res Solid Earth 122:9184–9207. https://doi.org/10.1002/2017JB014738
Fan W, McGuire J, de Groot-Hedlin C, Hedlin M, Coats S, Fiedler J (2019) Stormquakes. Geophys Res Lett 46:12909–12918. https://doi.org/10.1029/2019GL084217
Farra V, Stutzmann E, Gualtieri L, Schimmel M, Ardhuin F (2016) Ray-theoretical modeling of secondary microseism *P* waves. Geophys J Int 206:1730–1739
Friedrich A, Krüger F, Klinge K (1998) Ocean-generated microseismic noise located with the Gräfenberg array. J Seismol 2:47–64
Fukao Y, Nishida K, Kobayashi N (2010) Seafloor topography, ocean infragravity waves, and background Love and Rayleigh waves. J Geophys Res 115:B04302
Fukao Y, Nishida K, Suda N, Nawa K, Kobayashi N (2002) A theory of the Earth's background free oscillations. J Geophys Res 107:2206
Gal M, Reading AM, Ellingsen SP, Gualtieri L, Koper KD, Burlacu R, Tkalčić H, Hemer MA (2015) The frequency dependence and locations of short-period microseisms generated in the Southern Ocean and West Pacific. J Geophys Res Solid Earth 120:5764–5781. https://doi.org/10.1002/2015JB012210
Gerstoft P, Bromirski P (2016) Weather Bomb induced seismic signals. Science 353:869–870. https://doi.org/10.1126/science.aag1616
Gerstoft P, Fehler MC, Sabra KG (2006) When Katrina hit California. Geophys Res Letts 33(1):17308. https://doi.org/10.1029/2006GL027270
Gerstoft P, Shearer PM, Harmon N, Zhang J (2008) Global P, PP, and PKP wave microseisms observed from distant storms. Geophys Res Lett 35:4–9
Gerstoft P, Tanimoto T (2007) A year of microseisms in southern California. Geophys Res Lett 34:L20304. https://doi.org/10.1029/2007GL031091
Gilbert F (1970) Excitation of normal modes of the Earth by earthquake sources. Geophys J Roy Astron Soc 22:223–226
Gualtieri L, Bachmann E, Simons F, Tromp J (2020) The origin of secondary microseism Love waves. Proc Nat Acad Sci 117(47):29504–29511. https://doi.org/10.1073/pnas.2013806117
Gualtieri L, Stutzmann E, Capdeville Y, Farra V, Mangeney A, Morelli A (2015) On the shaping factors of the secondary microseismic wavefield. J Geophys Res 120:6241–6262
Gutenberg B (1912) Die seismische bodenunruhe (dissertation). Gerl Beitr Z Geophys 11:314–353
Gutenberg B (1936) On microseisms. Bull Seism Soc Am 26(2):111–117
Harmon N, Henstock T, Srokosz M, Tilmann F, Rietbrock A, Barton P (2012) Infragravity wave source regions determined from ambient noise correlation. Geophys Res Lett 39:1–5
Haubrich RA, McCamy K (1969) Microseisms: coastal and pelagic sources. Rev Geophys 7:539–571
Hasselmann K (1963) A statistical analysis of the generation of microseisms. Rev Geophys 1:177–210
Hetényi G, Molinari I, Clinton J et al (2018) The AlpArray Seismic Network: a large-scale European experiment to image the Alpine orogeny. Surv Geophys 39:1009–1033. https://doi.org/10.1007/s10712-018-9472-4
Herbers THC, Elgar S, Guza RT (1995) Generation and propagation of infragravity waves. J Geophys Res 100:24863–24872
Incorporated Research Institutions for Seismology (December 1984) Appendix 1A" (PDF), science plan for a new global seismographic Network, LCCN 84-82089
Janssen P (2004) The interaction of ocean waves and wind. Cambridge University Press, Cambridge
Juretzek C, Hadziioannou C (2016) Where do ocean microseisms come from? A study of Love-to-Rayleigh wave ratios. J Geophys Res 121:6741–6756
Kanamori H (1998) SEISMOLOGY: enhanced: shaking without quaking. Science 279:2063–2064
Kedar S, Longuet-Higgins M, Webb F, Graham N, Clayton R, Jones C (2008) The origin of deep ocean microseisms in the North Atlantic Ocean. Proc Roy Soc A 464:777–793
Kobayashi N, Nishida K (1998) Continuous excitation of planetary free oscillations by atmospheric disturbances. Nature 395:357–360
Koper KD, Burlacu R (2015) The fine structure of double-frequency microseisms recorded by seismometers in North America. J Geophys Res Solid Earth 120(3):1677–1691. https://doi.org/10.1002/2014JB011820
Kurrle D, Widmer-Schnidrig R (2008) The horizontal hum of the Earth: a global background of spheroidal and toroidal modes. Geophys Res Lett 35:1–5
Landès M, Hubans F, Shapiro NM, Paul A, Campillo M (2010) Origin of deep ocean microseisms by using teleseismic body waves. J Geophys Res 115:B05302
Lecocq T et al. (2020) Global quieting of high-frequency seismic noise due to COVID-19 pandemic lockdown measures. Science 136:1338–1343

Le Pape F, Craig D, Bean CJ (2021) How deep ocean-land coupling controls the generation of secondary microseism Love waves. Nat Commun 12(1):2332. https://doi.org/10.1038/s41467-021-22591-5
Liu Q, Koper KD, Burlacu R, Ni S, Wang F, Zou C, Wei Y, Gal M, Reading AM (2016) Source locations of teleseismic P, SV, and SH waves observed in microseisms recorded by a large aperture seismic array in China. Earth Planet Sci Lett 449:39–47
Longuet-Higgins MS (1950) A theory of the origin of microseisms. Proc Roy Soc A 243:1–35
Matsuzawa T, Obara K, Maeda T, Asano Y, Saito T (2012) Love- and Rayleigh-wave microseisms excited by migrating ocean swells in the North Atlantic detected in Japan and Germany. Bull Seismol Soc Am 102:1864–1871
Miche A (1944) Mouvements ondulatoires de la mer en profondeur croissante ou décroissante. Première partie. Mouvements ondulatoires périodiques et cylindriques en profondeur constante. Ann Ponts Chaussées 114:42–78
Mitchell ED, Vasiloff SV, Stumpf GJ, Witt A, Eilts MD, Johnson JT, Thomas KW (1998) The national severe storms laboratory tornado detection algorithm. Weather Forecast 13(2):352–366
Nawa K, Suda N, Fukao Y, Sato T, Aoyama Y, Shibuya K (1998) Incessant excitation of the Earth's free oscillations. Earth Planets Space 50:3–8
Neale J, Harmon N, Srokosz M (2017) Monitoring remote ocean waves using P-wave microseisms. J Geophys Res 122:470–483
Neale J, Harmon N, Srokosz M (2018) Monitoring remote ocean waves using p-wave microseisms. J Geophys Res Oceans 123(1):446–492. https://doi.org/10.1002/2016jc012183
Nishida K (2013) Earth's background free oscillations. Annu Rev Earth Planet Sci 41:719–740
Nishida K (2017) Ambient seismic wave field. Proc Jpn Acad Ser B 93(7):423–448. https://doi.org/10.2183/pjab.93.026
Nishida K, Fukao Y (2007) Source distribution of Earth's background free oscillations. J Geophys Res 112:B06306
Nishida K, Kawakatsu H, Fukao Y, Obara K (2008) Background Love and Rayleigh waves simultaneously generated at the Pacific Ocean floors. Geophys Res Lett 35:L16307
Nishida K, Kobayashi N, Fukao Y (2002) Origin of Earth's ground noise from 2 to 20 mHz. Geophys Res Lett 29:52-1–52-4
Nishida K, Takagi R (2016) Teleseismic S wave microseisms. Science 353:919–921
Nishida K, Takagi R (2022) A global centroid single force catalogue of P-wave microseisms. J Geophys Res Solid Earth 127:e2021jb023484. https://doi.org/10.1029/2021JB023484
Obara K (2003) Hi-net: High sensitivity seismograph network, Japan. In: Methods and applications of signal processing in seismic network operations. Lecture Notes in Earth Sciences, vol 98. Springer, Berlin. https://doi.org/10.1007/BFb0117698
Okada Y, Kasahara K, Hori S, Obara K, Sekiguchi S, Fujiwara H, Yamamoto A (2004) Recent progress of seismic observation networks in Japan: Hi-net, F-net, K-net, KiK-net. Earth Planets Space 56:15–18
Omori F (1918) On a relation between microseisms and ocean swell. Rep Imperial Earthq Inv Comm 89:12–18 (**(in Japanese)**)
Peterson J (1993) Observations and modeling of seismic background noise. U.S. Geol. Surv. Open File Rep. pp 93–322
Pyle ML, Koper KD, Euler GG, Burlacu R (2015) Location of high-frequency P wave microseismic noise in the Pacific Ocean using multiple small aperture arrays. Geophys Res Lett 42(8):2700–2708. https://doi.org/10.1002/2015GL063530
Rawat A, Ardhuin F, Ballu V, Crawford W, Corela C, Aucan J (2014) Infragravity waves across the oceans. Geophys Res Lett 41:7957–7963
Reading AM, Koper KD, Gal M, Graham LS, Tkalčić H, Hemer MA (2014) Dominant seismic noise sources in the Southern Ocean and West Pacific, 2000–2012, recorded at the Warramunga Seismic Array, Australia. Geophys Res Lett 41:3455–3463
Retailleau L, Gualtieri L (2021) Multi-phase seismic source imprint of tropical cyclones. Nat Commun 12(1):2064. https://doi.org/10.1038/s41467-021-22231-y
Rhie J, Romanowicz B (2004) Excitation of Earth's continuous free oscillations by atmosphere-ocean-seafloor coupling. Nature 431:552–556
Rhie J, Romanowicz B (2006) A study of the relation between ocean storms and the Earth's hum. Geochem Geophys Geosyst 7:Q10004
Roult G, Crawford W (2000) Analysis of 'background' free oscillations and how to improve resolution by subtracting the atmospheric pressure signal. Phys Earth Planet Inter 121:325–338
Saito T (2010) Love-wave excitation due to the interaction between a propagating ocean wave and the sea-bottom topography. Geophys J Int 182:1515–1523
Schulte-Pelkum V, Earle PS, Vernon FL (2004) Strong directivity of ocean-generated seismic noise. Geochem Geophys Geosyst 5:1–13
Sorrells GG (1971) A preliminary investigation into the relationship between long-period seismic noise and local fluctuations in the atmospheric pressure field. Geophys J Int 26(1–4):71–82. https://doi.org/10.1111/j.1365-246X.1971.tb03383.x
Sorrells G, MacDonald JA, Der ZA, Herrin E (1971) Earth motion caused by local atmospheric pressure changes. Geophys J Astron Soc 26:83–98
Sorrells G, Goforth T (1973) Low-frequency earth motion generated by slowly propagating partially organized pressure fields. Bull Seism Soc Am 63:1583–1601
Suda N, Nawa K, Fukao Y (1998) Earth's background free oscillations. Science 279:2089–2091
Talmadge C, Waxler R (2016) Infrasound from tornados: theory, measurement, and prospects for their use in early warning systems. Acoust Today 12:43–51
Tanimoto T (1999) Excitation of normal modes by atmospheric turbulence: source of long-period seismic noise. Geophys J Int 136:395–402
Tanimoto T (2001) Continuous free oscillations: atmosphere-solid earth coupling. Annu Rev Earth Planet Sci 29:563–584
Tanimoto T (2005) The oceanic excitation hypothesis for the continuous oscillations of the Earth. Geophys J Int 160:276–288. https://doi.org/10.1111/j.1365-246X.2004.02484.x
Tanimoto T (2007a) Excitation of normal modes by nonlinear interaction of ocean waves. Geophys J Int 168:571–582. https://doi.org/10.1111/j.1365-246X.2006.03240.x
Tanimoto T (2007b) Excitation of microseisms. Gephys Res Lett 34:L05308. https://doi.org/10.1029/2006GL029046
Tanimoto T (2010) Equivalent forces for colliding ocean waves. Geophys J Int 181:468–478. https://doi.org/10.1111/j.1365-246X.2010.04505.x
Tanimoto T, Heki K, Artru-Lambin J (2015a) Interaction of solid earth, atmosphere, and ionosphere. In: Gerald Schubert (editor-in-chief) treatise on geophysics, 2nd edn, vol 4. Elsevier, Oxford, pp 421–443
Tanimoto T, Ishimaru S, Alvizuri C (2006) Seasonality in particle motion of microseisms. Geophys J Int 166:253–266. https://doi.org/10.1111/j.1365-246X.2006.02931.x
Tanimoto T, Hadziioannou C, Igel H, Wassermann J, Schreiber U, Gebauer A (2015b) Estimate of Rayleigh-to-Love wave ratio in the secondary microseism by colocated ring laser and seismograph. Geophys Res Lett 42:2650–2655
Tanimoto T, Hadziioannou C, Igel H, Wassermann J, Schreiber U, Gebauer A, Chow B (2016a) Seasonal variations in the Rayleigh-to-Love wave ratio in the secondary microseism from colocated ring laser and seismograph. J Geophys Res 121:2447–2459
Tanimoto T, Lamontagne A (2014) Temporal and spatial evolution of an on-land hurricane observed by seismic data. Geophys Res Lett 41(21):7532–7538
Tanimoto T, Lin C-J, Hadziioannou C, Igel H, Vernon F (2016b) Estimate of Rayleigh-to- Love wave ratio in the secondary microseism by a small array at Piñon Flat observatory, California. Geophys Res Lett 43:173–181
Tanimoto T, Um J (1999) Cause of continuous oscillations of the Earth. J Geophys Res 104:28723–28739
Tanimoto T, Um J, Nishida K, Kobayashi N (1998) Earth's continuous oscillations observed on seismically quiet days. Geophys Res Lett 25:1553–1556
Tanimoto T, Valovcin A (2015) Stochastic excitation of seismic waves by a hurricane. J Geophys Res Solid Earth 120(11):7713–7728
Tanimoto T, Wang J (2018) Low-frequency seismic noise characteristics from the analysis of co-located seismic and pressure data. J Geophys Res Solid Earth 123(7):5853–5885. https://doi.org/10.1029/2018JB015519
Tanimoto T, Wang J (2019) Theory for deriving shallow elasticity structure from co-located seismic and pressure data. J Geophys Res Solid Earth 124(6):5811–5835. https://doi.org/10.1029/2018JB017132
Tanimoto T, Wang J (2020) Shallow elasticity structure from colocated pressure and seismic stations in the Piñon Flat Observatory and estimation of

Vs30. Geophys J Int 222(1):678–696. https://doi.org/10.1093/gji/ggaa195
Tanimoto T, Wang J (2021) Incorporating wind information in the inversion of co-located pressure and seismic data for shallow elastic structure. J Geophys Res Solid Earth. https://doi.org/10.1029/2020JB021162
Tatom F, Vitton S (2001) The transfer of energy from a tornado into the ground. Seismol Res Lett 72:12–21
Tatom F, Knupp K, Vitton S (1995) Tornado detection based on seismic signal. J Appl Meteorol 34:572–582
Toksöz MN, Lacoss RT (1968) Microseisms: mode structure and sources. Science 159:872–873
Traer J, Gerstoft P, Bromirski PD, Shearer PM (2012) Microseisms and hum from ocean surface gravity waves. J Geophys Res 117:B11307
Uchiyama Y, McWilliams JC (2008) Infragravity waves in the deep ocean: generation, propagation, and seismic hum excitation. J Geophys Res 113:1–25
Valovcin A, Tanimoto T (2017) Modeling the excitation of seismic waves by the Joplin tornado. Geophys Res Lett 44:10256–10261. https://doi.org/10.1002/2017GL074185
Wang J, Tanimoto T (2020) Estimating near-surface rigidity from low-frequency noise using collocated pressure and horizontal seismic data. Bull Seismol Soc Am 20:1–11. https://doi.org/10.1785/0120200098
Wang J, Tanimoto T (2022) Estimation of Vs30 at the EarthScope transportable array stations by inversion of low-frequency seismic noise. J Geophys Res 127:e2021JB023469. https://doi.org/10.1029/2021JB023469
Warburton RJ, Goodkind JM (1977) The influence of barometric-pressure variations on gravity. Geophys J Roy Astron Soc 48:281–292
Watada S, Masters G (2001) Oceanic excitation of the continuous oscillations of the earth. In: Eos Transactions AGU 82, SS2A-0620
Webb SC (2008) The Earth's hum: the excitation of Earth normal modes by ocean waves. Geophys J Int 174:542–566
Webb SC, Zhang X, Crawford W (1991) Infragravity waves in the deep ocean. J Geophys Res 96:2723–2736
Webb S, Crawford W (1999) Long-period seafloor seismology and deformation under ocean waves. Bull Seism Soc Am 89:1535–1542
Wiechert E (1904) Discussion, Verhandlung der zweiten internationalen seismologischen Konfer- enz. Beitr Geophys 2:41–43
Xiao H, Eilon ZC, Ji C, Tanimoto T (2020) COVID-19 Societal Response Captured by Seismic Noise in China and Italy. Seismol Res Lett 20:1–12. https://doi.org/10.1785/0220200147
Xiao H, Tanimoto T, Spica ZJ, Gaite B, Ruiz-Barajas S, Pan M, Viens L (2022) Locating the precise sources of high-frequency microseisms using distributed acoustic sensing. Geophys Res Lett 49:e2022GL099292. https://doi.org/10.1029/2022GL099292
Xiao H, Tanimoto T, Xue M (2021) Study of S-wave microseisms generated by storms in the Southeast Australia and North Atlantic. Geophys Res Lett 48:e2021GL093728. https://doi.org/10.1029/2021GL093728
Young IR (1999) Wind generated ocean waves, Elsevier Ocean Engineering Book Serles, vol 2. Elsevier, New York
Zhang J, Gerstoft P, Bromirski PD (2010) Pelagic and coastal sources of P-wave microseisms: generation under tropical cyclones. Geo- Phys Res Lett 37:1–6
Zhang J, Gerstoft P, Shearer P (2009) High-frequency P-wave seismic noise driven by ocean winds. Geophys Res Lett 36:L09302. https://doi.org/10.1029/2009GL037761
Zürn W, Widmer R (1995) On noise reduction in vertical seismic records below 2 mHz using local barometric pressure. Geophys Res Lett 22:3537–3540

Publisher's Note